Nonlinear optical phenomena in silicon waveguides: Modeling and applications

Q. Lin,[1,*] **Oskar J. Painter,**[1] **and Govind P. Agrawal**[2]

[1]*Department of Applied Physics, California Institute of Technology, Pasadena, CA 91125*
[2]*Institute of Optics, University of Rochester, Rochester, NY 14627*
linq@caltech.edu

Abstract: Several kinds of nonlinear optical effects have been observed in recent years using silicon waveguides, and their device applications are attracting considerable attention. In this review, we provide a unified theoretical platform that not only can be used for understanding the underlying physics but should also provide guidance toward new and useful applications. We begin with a description of the third-order nonlinearity of silicon and consider the tensorial nature of both the electronic and Raman contributions. The generation of free carriers through two-photon absorption and their impact on various nonlinear phenomena is included fully within the theory presented here. We derive a general propagation equation in the frequency domain and show how it leads to a generalized nonlinear Schrödinger equation when it is converted to the time domain. We use this equation to study propagation of ultrashort optical pulses in the presence of self-phase modulation and show the possibility of soliton formation and supercontinuum generation. The nonlinear phenomena of cross-phase modulation and stimulated Raman scattering are discussed next with emphasis on the impact of free carriers on Raman amplification and lasing. We also consider the four-wave mixing process for both continuous-wave and pulsed pumping and discuss the conditions under which parametric amplification and wavelength conversion can be realized with net gain in the telecommunication band.

OCIS codes: (190.5970) Semiconductor nonlinear optics; (130.3120) Integrated optics devices; (250.4390) Nonlinear optics, integrated optics; (320.7110) Ultrafast nonlinear optics

References and links

1. L. Pavesi and D. J. Lockwood, Eds., *Silicon Photonics* (Springer, New York, 2004).
2. G. T. Reed and A. P. Knights, *Silicon Photonics: An Introduction* (Wiley, Hoboken, NJ, 2004).
3. R. A. Soref, "The Past, Present, and Future of Silicon Photonics," IEEE J. Sel. Top. Quantum Electron. **12**, 1678–1687 (2006).
4. R. A. Soref, S. J. Emelett, and W. R. Buchwald, "Silicon waveguided components for the long-wave infrared region," J. Opt. A: Pure Appl. Opt. **8**, 840–848 (2006).
5. M. Dinu, F. Quochi, and H. Garcia, "Third-order nonlinearities in silicon at telecom wavelengths," Appl. Phys. Lett. **82**, 2954–2956 (2003).
6. R. Claps, D. Dimitropoulos, V. Raghunathan, Y. Han, and B. Jalali, "Observation of stimulated Raman amplification in silicon waveguides," Opt. Express **11**, 1731–1739 (2003).
7. H. K. Tsang, C. S. Wong, T. K. Liang, I. E. Day, S. W. Roberts, A. Harpin, J. Drake, and M. Asghari, "Optical dispersion, two-photon absorption, and self-phase modulation in silicon waveguides at 1.5 μm wavelength," Appl. Phys. Lett. **80**, 416–418 (2002).

#88416 - $15.00 USD Received 9 Oct 2007; revised 22 Nov 2007; accepted 25 Nov 2007; published 29 Nov 2007

8. O. Boyraz, T. Indukuri, and B. Jalali, "Self-phase-modulation induced spectral broadening in silicon waveguides," Opt. Express **12**, 829–834 (2004).
9. G. W. Rieger, K. S. Virk, and J. F. Yong, "Nonlinear propagation of ultrafast 1.5 μm pulses in high-index-contrast silicon-on-insulator waveguides," Appl. Phys. Lett. **84**, 900–902 (2004).
10. A. R. Cowan, G. W. Rieger, and J. F. Young, "Nonlinear transmission of 1.5 μm pulses through single-mode silicon-on-insulator waveguide structures," Opt. Express **12**, 1611–1621 (2004).
11. H. Yamada, M. Shirane, T. Chu, H. Yokoyama, S. Ishida, and Y. Arakawa, "Nonlinear-optic silicon-nanowire waveguides," Jap. J. Appl. Phys. **44**, 6541–6545 (2005).
12. E. Dulkeith, Y. A. Vlasov, X. Chen, N. C. Panoiu, and R. M. Osgood, Jr., "Self-phase-modulation in submicron silicon-on-insulator photonic wires," Opt. Express **14**, 5524–5534 (2006).
13. L. Yin, Q. Lin, and G. P. Agrawal, "Dispersion tailoring and soliton propagation in silicon waveguides," Opt. Lett. **31**, 1295–1297 (2006).
14. R. Dekker, A. Driessen, T. Wahlbrink, C. Moormann, J. Niehusmann, and M. Först, "Ultrafast Kerr-induced all-optical wavelength conversion in silicon waveguides using 1.55 μm femtosecond pulses," Opt. Express **14**, 8336–8346 (2006).
15. I-W. Hsieh, X. Chen, J. I. Dadap, N. C. Panoiu, R. M. Osgood, Jr., S. J. McNab, and Y. A. Vlasov, "Ultrafast-pulse self-phase modulation and third-order dispersion in Si photonic wire-waveguides," Opt. Express **14**, 12380–12387 (2006).
16. L. Yin, Q. Lin, and G. P. Agrawal, "Soliton fission and supercontinuum generation in silicon waveguides," Opt. Lett. **32**, 391–393 (2007).
17. J. Zhang, Q. Lin, G. Piredda, R. W. Boyd, G. P. Agrawal, and P. M. Fauchet, "Optical solitons in a silicon waveguide," Opt. Express **15**, 7682–7688 (2007).
18. P. Koonath, D. R. Solli, and B. Jalali, "Continuum generation and carving on a silicon chip," Appl. Phys. Lett. **91**, 061111 (2007).
19. R. Salem, M. A. Foster, A. C. Turner, D. F. Geraghty, M. Lipson, and A. L. Gaeta, "All-optical regeneration on a silicon chip," Opt. Express **15**, 7802–7809 (2007).
20. R. Dekker, N. Usechak, M. Först, and A. Driessen, "Ultrafast nonlinear all-optical processes in silicon-on-insulator waveguides," J. Phys. D: Appl. Phys. **40**, R249–R271 (2007).
21. L. Yin and G. P. Agrawal, "Impact of two-photon absorption on self-phase modulation in silicon waveguides," Opt. Lett. **32**, 2031–2033 (2007).
22. N. Suzuki, "FDTD analysis of two-photon absorption and free-carrier absorption in Si high-index-contrast waveguides," J. Lightwave Technol. **25**, 2495–2501 (2007).
23. I-W. Hsieh, X. Chen, X. Liu, J. I. Dadap, N. C. Panoiu, C-Y. Chou, F. Xia, W. M. Green, Y. A. Vlasov, and R. M. Osgood, Jr., "Supercontinuum generation in silicon photonic wires," Opt. Express **15**, 15242–15248 (2007).
24. A. Hache and M. Bourgeois, "Ultrafast all-optical switching in a silicon-based photonic crystal," Appl. Phys. Lett. **77**, 4089–4091 (2000).
25. Ö. Boyraz, P. Koonath, V. Raghunathan, and B. Jalali, "All optical switching and continuum generation in silicon waveguides," Opt. Express **12**, 4094–4102 (2004).
26. I-W. Hsieh, X. Chen, J. I. Dadap, N. C. Panoiu, R. M. Osgood, Jr., S. J. McNab, and Y. A. Vlasov, "Cross-phase modulation-induced spectral and temporal effects on co-propagating femtosecond pulses in silicon photonic wires," Opt. Express **15**, 1135–1146 (2007).
27. R. Claps, D. Dimitropoulos, Y. Han, and B. Jalali, "Observation of Raman emission in silicon waveguide at 1.54 μm," Opt. Express **10**, 1305–1313 (2002).
28. D. Dimitropoulos, B. Houshmand, R.Claps, and B. Jalali, "Coupled-mode theory of the Raman effect in silicon-on-insulator waveguides," Opt. Lett. **28**, 1954–1956 (2003).
29. J. I. Dadap, R. L. Espinola, R. M. Osgood, Jr., S. J. McNab, and Y. A. Vlasov, "Spontaneous Raman scattering in ultrasmall silicon waveguides," Opt. Lett. **29**, 2755–2757 (2004).
30. R. L. Espinola, J. I. Dadap, R. M. Osgood, Jr., S. J. McNab, and Y. A. Vlasov, "Raman amplification in ultrasmall silicon-on-insulator wire waveguides," Opt. Express **12**, 3713–3718 (2004).
31. Q. Xu, V. R. Almeida, and M. Lipson, "Time-resolved study of Raman gain in highly confined silicon-on-insulator waveguides," Opt. Express **12**, 4437–4442 (2004).
32. A. Liu, H. Rong, M. Paniccia, O. Cohen, and D. Hak, "Net optical gain in a low loss silicon-on-insulator waveguide by stimulated Raman scattering," Opt. Express **12**, 4261–4268 (2004).
33. H. Rong, A. Liu, R. Nicolaescu, M. Paniccia, O. Cohen, and D. Hak, "Raman gain and nonlinear optical absorption measurement in a low-loss silicon waveguide," Appl. Phys. Lett. **85**, 2196–2198 (2004).
34. T. K. Liang and H. K. Tsang, "Efficient Raman amplificationin silicon-on-insulator waveguides," Appl. Phys. Lett. **85**, 3343–3345 (2004).
35. T. K. Liang and H. K. Tsang, "Role of free carriers from two-photon absorption in Raman amplification in silicon-on-insulator waveguides," Appl. Phys. Lett. **84**, 2745–2747 (2004).
36. R. Claps, V. Raghunathan, D. Dimitropoulos, and B. Jalali, "Influence of nonlinear absorption on Raman amplification in silicon waveguides," Opt. Express **12**, 2774–2780 (2004).
37. T. K. Liang and H. K. Tsang, "Nonlinear absorption and Raman scattering in silicon-on-insulator optical

#88416 - $15.00 USD Received 9 Oct 2007; revised 22 Nov 2007; accepted 25 Nov 2007; published 29 Nov 2007

waveguides," IEEE J. Quantum Electron. **10**, 1149–1153 (2004).
38. O. Boyraz and B. Jalali, "Demonstration of a silicon Raman laser," Opt. Express **12**, 5269–5273 (2004).
39. M. Krause, H. Renner, and E. Brinkmeyer, "Analysis of Raman lasing characteristics in silicon-on-insulator waveguides," Opt. Express **12**, 5703–5710 (2004).
40. Q. Xu, V. R. Almeida, and M. Lipson, "Demonstration of high Raman gain in a submicrometer-size silicon-on-insulator waveguide," Opt. Lett. **30**, 35–37 (2005).
41. H. Rong, A. Liu, R. Jones, O. Cohen, D. Hak, R. Nicolaescu, A. Fang, and M. Paniccia, "An all-silicon Raman laser," Nature **433**, 292–294 (2005).
42. H. Rong, R. Jones, A. Liu, O. Cohen, D. Hak, A. Fang, and M. Paniccia, "A continuous-wave Raman silicon laser," Nature **433**, 725–728 (2005).
43. O. Boyraz and B. Jalali, "Demonstration of directly modulated silicon Raman laser," Opt. Express **13**, 796–800 (2005).
44. V. Raghunathan, O. Boyraz, ann B. Jalali, "20 dB on-off Raman amplification in silicon waveguides," Proc. Conf. Lasers Electro-Optics (OSA, Washington, DC, 2005), pp. 349–351.
45. R. Jones, A. Liu, H. Rong, M. Paniccia, O. Cohen, and D. Hak, "Lossless optical modulation in a silicon waveguide using stimulated Raman scattering," Opt. Express **13**, 1716–1723 (2005).
46. X. Yang and C. W. Wong, "Design of photonic band gap nanocavities for stimulated Raman amplification and lasing in monolithic silicon," Opt. Express **13**, 4723–4730 (2005).
47. X. Chen, N. C. Panoiu, R. M. Osgood, Jr., "Theory of Raman-mediated pulsed amplification in silicon-wire waveguides," IEEE J. Quantum Electron. **42**, 160–170 (2006).
48. V. M. N. Passaro and F. D. Leonardis, "Space-time modeling of Raman pulses in silicon-on-insulator optical waveguides," IEEE J. Lightwave Technol. **24**, 2920–2931 (2006).
49. J. F. McMillan, X. Yang, N. C. Panoiu, R. M. Osgood, and C. W. Wong, "Enhanced stimulated Raman scattering in slow-light photonic crystal waveguides," Opt. Lett. **31**, 1235–1237 (2006).
50. S. Blair and K. Zheng, "Intensity-tunable group delay using stimulated Raman scattering in silicon slow-light waveguides," Opt. Express **14**, 1064–1069 (2006).
51. Y. Okawachi, M. A. Foster, J. E. Sharping, A. L. Gaeta, Q. Xu, and M. Lipson, "All-optical slow-light on a photonic chip," Opt. Express **14**, 2317–2322 (2006).
52. A. Liu, H. Rong, R. Jones, O. Cohen, D. Hak, and M. Paniccia, "Optical amplification and lasing by stimulated Raman scattering in silicon waveguides," IEEE J. Lightwave Technol. **24**, 1440–1455 (2006).
53. B. Jalali, V. Raghunathan, D. Dimitropoulos, and O. Boyraz, "Raman-based silicon photonics," IEEE J. Sel. Top. Quantum Electron. **12**, 412–421 (2006).
54. H. Rong, S. Xu, Y. Kuo, V. Sih, O. Cohen, O. Raday, and M. Paniccia, "Low-threshold continuous-wave Raman silicon laser," Nature Photon. **1**, 232–237 (2007).
55. X. Yang and C. W. Wong, "Coupled-mode theory for stimulated Raman scattering in high-Q/V_m silicon photonic band gap defect cavity lasers," Opt. Express **15**, 4763–4780 (2007).
56. V. Sih, S. Xu, Y. Kuo, H. Rong, M. Paniccia, O. Cohen, and O. Raday, "Raman amplification of 40 Gb/s data in low-loss silicon waveguides," Opt. Express **15**, 357–362 (2007).
57. V. Raghunathan, H. Renner, R. R. Rice, and B. Jalali, "Self-imaging silicon Raman amplifier," Opt. Express **15**, 3396–3408 (2007).
58. F. De Leonardis and V. M. N. Passaro, "Modelling of Raman amplification in silicon-on-insulator optical microcavities," New J. Phys. **9**, 25 (2007).
59. F. De Leonardis and V. M. N. Passaro, "Modeling and performance of a guided-wave optical angular-velocity sensor based on Raman effect in SOI," IEEE J. Lightwave Technol. **25**, 2352–2366 (2007).
60. V. Raghunathan, D. Borlaug, R. R. Rice, and B. Jalali, "Demonstration of a mid-infrared silicon Raman amplifier," Opt. Express **15**, 14355–14362 (2007).
61. R. Claps, V. Raghunathan, D. Dimitropoulos, and B. Jalali, "Anti-Sotkes Raman conversion in silicon waveguides," Opt. Express **11**, 2862–2872 (2003).
62. D. Dimitropoulos, V. Raghunathan, R. Claps, and B. Jalali, "Phase-matching and nonlinear optical processes in silicon waveguides," Opt. Express **12**, 149–160 (2003).
63. V. Raghunathan, R. Claps, D. Dimitropoulos, and B. Jalali, "Wavelength conversion in silicon using Raman induced four-wave mixing," Appl. Phys. Lett. **85**, 34–26 (2004).
64. R. L. Espinola, J. I, Dadap, R. M. Osgood, Jr., S. J. McNab, and Y. A. Vlasov, "C-band wavelength conversion in silicon photonic wire waveguides," Opt. Express **13**, 4341–4349 (2005).
65. H. Fukuda, K. Yamada, T. Shoji, M. Takahashi, T. Tsuchizawa, T. Watanabe, J. Takahashi, and S. Itabashi, "Four-wave mixing in silicon wire waveguides," Opt. Express **13**, 4629–4637 (2005).
66. V. Raghunathan, R. Claps, D. Dimitropoulos, and B. Jalali, "Parametric Raman wavelength conversion in scaled silicon waveguides," IEEE J. Lightwave Technol. **23**, 2094–2102 (2005).
67. H. Rong, Y. Kuo, A. Liu, M. Paniccia, and O. Cohen, "High efficiency wavelength conversion of 10 Gb/s data in silicon waveguides," Opt. Express **14**, 1182–1188 (2006).
68. Q. Lin, J. Zhang, P. M. Fauchet, and G. P. Agrawal, "Ultrabroadband parametric generation and wavelength conversion in silicon waveguides," Opt. Express **14**, 4786–4799 (2006).

#88416 - $15.00 USD Received 9 Oct 2007; revised 22 Nov 2007; accepted 25 Nov 2007; published 29 Nov 2007

69. M. A. Foster, A. C. Turner, J. E. Sharping, B. S. Schmidt, M. Lipson, and A. L. Gaeta, "Broad-band optical parametric gain on a silicon photonic chip," Nature **441**, 960–963 (2006).
70. D. Dimitropoulos, D. R. Solli, R. Claps, and B. Jalali, "Noise figure and photon statistics in coherent anti-Stokes Raman scattering," Opt. Express **14**, 11418–11432 (2006).
71. K. Yamada, H. Fukuda, T. Tsuchizawa, T. Watanabe, T. Shoji, and S. Itabashi, "All-optical efficient wavelength conversion using silicon photonic wire waveguide," IEEE Photon. Technol. Lett. **18**, 1046–1048 (2006).
72. Y. Kuo, H. Rong, V. Sih, S. Xu, M. Paniccia, and O. Cohen, "Demonstration of wavelength conversion at 40 Gb/s data rate in silicon waveguides," Opt. Express **14**, 11721–11726 (2006).
73. Q. Lin and G. P. Agrawal, "Silicon waveguides for creating quantum-correlated photon pairs," Opt. Lett. **31**, 3140–3142 (2006).
74. N. C. Panoiu, X. Chen, and R. M. Osgood, Jr., "Modulation instability in silicon photonic nanowires," Opt. Lett. **31**, 3609–3611 (2006).
75. J. E. Sharping, K. F. Lee, M. A. Foster, A. C. Turner, B. S. Schmidt, M. Lipson, A. L. Gaeta, and P. Kumar, "Generation of correlated photons in nanoscale silicon waveguides," Opt. Express **14**, 12388–12393 (2006).
76. N. Vermeulen, C. Debaes, and H. Thienpont, "Mitigating heat dissipation in near- and mid-infrared silicon-based Raman lasers using CARS," IEEE J. Sel. Top. Quantum Electron. **13**, 770–787 (2007).
77. A. C. Turner, M. A. Foster, A. L Gaeda, and M. Lipson, "Ultra-low power frequency conversion in silicon micro-ring resonators," Proc. Conf. Lasers Electro-Optics (OSA, Washington, DC, 2007), paper CPDA3.
78. S. Ayotte, H. Rong, S. Xu, O. Cohen, and M. Paniccia, "Multichannel dispersion compensation using a silicon waveguide-based optical phase conjugator," Opt. Lett. **32**, 2393–2395 (2007).
79. M. A. Foster, A. C. Turner, R. Salem, M. Lipson, and A. L. Gaeta, "Broad-band continuous-wave parametric wavelength conversion in silicon nanowaveguides," Opt. Express **15**, 12949–12958 (2007).
80. G. P. Agrawal, *Nonlinear Fiber Optics*, 4th ed. (Academic Press, Boston, 2007).
81. R. A. Soref and B. R. Bennett, "Electrooptical effects in silicon," IEEE J. Quantum Electron. **23**, 123–129 (1987).
82. V. Raghunathan, R. Shori, O. M. Stafsudd, B. Jalali, "Nonlinear absorption in silicon and the prospects of mid-infrared silicon Raman lasers," Physica Status Solidi A **203**, R38–R40 (2006).
83. A. D. Bristow, N. Rotenberg, and H. M. van Driel, "Two-photon absorption and Kerr coefficients of silicon for 850-2200 nm," Appl. Phys. Lett. **90**, 191104 (2007).
84. Q. Lin, J. Zhang, G. Piredda, R. W. Boyd, P. M. Fauchet, and G. P. Agrawal, "Dispersion of silicon nonlinearities in the near-infrared region," Appl. Phys. Lett. **90**, 021111 (2007).
85. M. Foster and A. L. Gaeta, "Wavelength dependence of the ultrafast third-order nonlinearity of Silicon," Proc. Conf. Lasers Electro-Optics (OSA, Washington, DC, 2007), Paper CTuY5.
86. D. J. Moss, H. M. van Driel, and J. E. Sipe, "Dispersion in the anisotropy of optical third-harmonic generation in silicon," Opt. Lett. **14**, 57–59 (1989).
87. J. Zhang, Q. Lin, G. Piredda, R. W. Boyd, G. P. Agrawal, and P. M. Fauchet, "Anisotropic nonlinear response of silicon in the near-infrared region," Appl. Phys. Lett. **90**, 071113 (2007).
88. P. E. Barclay, K. Srinivasan, and O. Painter, "Nonlinear response of silicon photonic crystal microresonators excited via an integrated waveguide and fiber taper", Opt. Express **13**, 801-820 (2005).
89. T. J. Johnson, M. Borselli, and O. Painter, "Self-induced optical modulation of the transmission through a high-Q silicon microdisk resonator", Opt. Express **14**, 817-831 (2006).
90. V. R. Almeida, C. A. Barrios, R. R. Panepucci, and M. Lipson, "All-optical control of light on a silicon chip," Nature **431**, 1081–1084 (2004).
91. T. Tanabe, M. Notomi, S. Mitsugi, A. Shinya, and E. Kuramochi, "All-optical switches on a silicon chip realized using photonic crystal nanocavities," Appl. Phys. Lett. **87**, 151112 (2005).
92. S. F. Preble, Q. Xu, B. S. Schmidt, and M. Lipson, "Ultrafast all-optical modulation on a silicon chip," Opt. Lett. **30**, 2891–2893 (2005).
93. T. G. Eusera and W. L. Vos, "Spatial homogeneity of optically switched semiconductor photonic crystals and of bulk semiconductors," J. Appl. Phys. **97**, 043102 (2005).
94. C. Manolatou and M. Lipson, "All-optical silicon modulators based on carrier injection by two-photon absorption," IEEE J. Lightwave Technol. **24**, 1433–1439 (2006).
95. F. Gan, F. J. Grawert, J. M. Schley, S. Akiyama, J. Michel, K. Wada, L. C. Kimerling, and F. X. Kärtner, "Design of all-optical switches based on carrier injection in Si/SiO_2 split-ridge waveguides (SRWs)," IEEE J. Lightwave Technol. **24**, 3454–3463 (2006).
96. K. Ikeda and Y. Fainman, "Nonlinear Fabry-Perot resonator with a silicon photonic crystal waveguide," Opt. Lett. **31**, 3486–3488 (2006).
97. E. Tien, N. S. Yuksek, F. Qian, and O. Boyraz, "Pulse compression and modelocking by using TPA in silicon waveguides," Opt. Express **15**, 6500–6506 (2007).
98. T. K. Liang, L. R. Nunes, T. Sakamoto, K. Sasagawa, T. Kawanishi, M. Tsuchiya, G. R. A. Priem, D. Van Thourhout, P. Dumon, R. Baets, and H. K. Tsang, "Ultrafast all-optical switching by cross-absorption modulation in silicon wire waveguides," Opt. Express **13**, 7298–7303 (2005).
99. D. J. Moss, L. Fu, I. Littler, and B. J. Eggleton, "Ultrafast all-optical modulation via two-photon absorption in

#88416 - $15.00 USD Received 9 Oct 2007; revised 22 Nov 2007; accepted 25 Nov 2007; published 29 Nov 2007

silicon-on-insulator waveguides," Electron. Lett. **41**, 320–321 (2005).
100. T. K. Liang, L. R. Nunes, M. Tsuchiya, K. S. Abedin, T. Miyazaki, D. Van Thourhout, W. Bogaerts, P. Dumon, R. Baets, and H. K. Tsang, "High speed logic gate using two-photon absorption in silicon waveguides," Opt. Commun. **265**, 171–174 (2006).
101. J. M. Dudley, G. Genty, and S. Coen, "Supercontinuum generation in photonic crystal fiber," Rev. Mod. Phys. **78**, 1135–1184 (2006).
102. P. N. Butcher and D. Cotter, *The Elements of Nonlinear Optics* (Cambridge University Press, New York, 1991).
103. R. W. Boyd, *Nonlinear Optics*, 2nd ed. (Academic Press, Boston, 2003).
104. Y. R. Shen and N. Bloembergen, "Theory of stimulated Brillouin and Raman scattering," Phys. Rev. **137**, A1787–A1805 (1965).
105. M. D. Lvenson and N. Bloembergen, "Dispersion of the nonlinear optical susceptibility tensor in centrosymmetric media," Phys. Rev. B **10**, 4447–4463 (1974).
106. M. Cardona, "Resonance phenomena," in *Light Scattering in Solid II*, M. Cardona and G. Güntherodt eds. (Springer-Verlag, New York, 1982).
107. R. H. Stolen, J. P. Gordon, W. J. Tomlinson, and H. A. Haus, "Raman response function of silica-core fibers," J. Opt. Soc. Am. B **6**, 1159–1166 (1989).
108. P. A. Temple and C. E. Hathaway, "Multiphonon Raman spectrum of silicon," Phys. Rev. B **7**, 3685–3697 (1973).
109. T. R. Hart, R. L. Aggarwal, and B. Lax, "Temperature dependence of Raman scattering in silicon," Phys. Rev. B **1**, 638–642 (1970).
110. A. Zwick and R. Carles, "Multiple-order Raman scattering in crystalline and amorphous silicon," Phys. Rev. B **48**, 6024–6032 (1993).
111. R. Loudon, "The Raman effect in crystals," Adv. Phys. **50**, 813–864 (2001).
112. J. R. Sandercock, "Brillouin-scattering measurements on silicon and germanium," Phys. Rev. Lett. **28**, 237–240 (1972).
113. M. Dinu, "Dispersion of phonon-assisted nonresonant third-order nonlinearities," IEEE J. Quantum Electron. **39**, 1498–1503 (2003).
114. H. Garcia and R. Kalyanaraman, "Phonon-assisted two-photon absorption in the presence of a dc-field: the nonlinear Franz-Keldysh effect in indirect gap semiconductor," J. Phys. B **39**, 2737–2746 (2006).
115. M. Sheik-Bahae and E. W. Van Stryland, "Optical nonlinearities in the transparency region of bulk semiconductors," in *Nonlinear Optics in Semiconductors I*, E. Garmire and A. Kost, Eds., *Semiconductors and Semimetals*, vol. 58 (Academic, Boston, 1999).
116. G. P. Agrawal, *Applications of Nonlinear Fiber Optics*, 2nd ed. (Academic Press, Boston, 2007).
117. R. W. Hellwarth, "Third-order optical susceptibilities of liquids and solids," Prog. Quantum Electron. **5**, 1–68 (1977).
118. P. D. Maker and R. W. Terhune, "Study of optical effects due to an induced polarization third order in the electric field strength," Phys. Rev. **137**, A801–A818 (1965).
119. S. S. Jha and N. Bloembergen, "Nonlinear optical susceptibilities in group-IV and III-V semiconductors," Phys. Rev. **171**, 891–898 (1968).
120. J. J. Wynne, "Optical third-order mixing in GaAs, Ge, Si, and InAs," Phys. Rev. **178**, 1295–1303 (1969).
121. R. Buhleier, G. Lüpke, G. Marowsky, Z. Gogolak, and J. Kuhl, "Anisotropic interference of degenerate four-wave mixing in crystalline silicon," Phys. Rev. B **50**, 2425–2431 (1994).
122. W. K. Burns and N. Bloembergen, "Third-harmonic generation in absorbing media of cubic or isotropic symmetry," Phys. Rev. B **4**, 3437–3450 (1971).
123. D. J. Moss, H. M. van Driel, and J. E. Sipe, "Third harmonic generation as a structure diagonostic of ion-implanted amorphous and crystalline silicon," Appl. Phys. Lett. **48**, 1150-1152 (1986).
124. C. C. Wang, J. Bomback, W. T. Donlon, C. R. Huo, and J. V. James, "Optical third-harmonic generation in reflection from crystalline and amorphous samples of silicon," Phys. Rev. Lett. **57**, 1647–1650 (1986).
125. D. J. Moss, E. Ghahramani, J. E. Sipe, and H. M. van Driel, "Band-structure calculation of dispersion and anisotropy in $\chi^{(3)}$ for third-harmonic generation in Si, Ge, and GaAs," Phys. Rev. B **41**, 1542–1560 (1990).
126. J. F. Reintjes and J. C. McGroddy, "Indirect two-photon transition in Si at 1.06 μm", Phys. Rev. Lett. **30**, 901–903 (1973).
127. V. Mizrahi, K. W. DeLong, G. I. Stegeman, M. A. Saifi, and M. J. Andrejco, "Two-photon absorption as a limitation to all-optical switching," Opt. Lett. **14**, 1140–1142 (1989).
128. M. Sheik-Bahae, D. C. Hutchings, D. J. Hagan, and E. W. Van Stryland, "Dispersion of bound electronic nonlinear refraction in solids," IEEE J. Quantum Electron. **27**, 1296–1309 (1991).
129. R. Salem and T. E. Murphy, "Polarization-insensitive cross correlation using two-photon absorption in a silicon photodiode," Opt. Lett. **29**, 1524–1526 (2004).
130. T. Kagawa and S. Ooami, "Polarization dependence of two-photon absorption in Si avalanche photodiodes," Jap. J. Appl. Phys. **46**, 664–668 (2007).
131. S. M. Sze and K. K. Ng, *Physics of Semiconductor Devices*, 3rd ed. (Wiley, Hoboken, NJ, 2007).
132. A. Othonos, "Probing ultrafast carrier and phonon dynamics in semiconductors," J. Appl. Phys. **83**, 1789–1830 (1998), and references therein.

#88416 - $15.00 USD Received 9 Oct 2007; revised 22 Nov 2007; accepted 25 Nov 2007; published 29 Nov 2007

133. A. J. Sabbah and D. M. Riffe, "Femtosecond pump-probe reflectivity study of silicon carrier dynamics," Phys. Rev. B **66**, 165217 (2002).
134. A. Kost, "Resonant optical nonlinearities in semiconductors," in *Nonlinear Optics in Semiconductors I*, E. Garmire and A. Kost, Eds., *Semiconductors and Semimetals*, vol. 58 (Academic, Boston, 1999).
135. R. A. Soref and B. R. Bennett, "Kramers-Kronig analysis of electro-optical switching in silicon," Proc. SPIE **704**, 32–37 (1987).
136. D. S. Chemla, "Ultrafast transient nonlinear optical processes in semiconductors," in *Nonlinear Optics in Semiconductors I*, E. Garmire and A. Kost, Eds., *Semiconductors and Semimetals*, vol. 58 (Academic, Boston, 1999).
137. Q. Lin, T. Johnson, R. Perahia, C. Michael, and O. J. Painter, "Highly tunable optical parametric oscillation in silicon micro-resonators," submitted for publication.
138. M. J. Adams, S. Ritchie, and M. J. Robertson, "Optimum overlap of electric and optical fields in semiconductor waveguide devices," Appl. Phys. Lett. **18**, 820–822 (1986).
139. D. Dimitropoulos, R. Jhaveri, R. Claps, J. C. S. Woo, and B. Jalali, "Lifetime of photogenerated carriers in silicon-on-insulator rib waveguides," Appl. Phys. Lett. **86**, 071115 (2005).
140. Y. Liu and H. K. Tsang, "Nonlinear absorption and Raman gain in helium-ion-implanted silicon waveguides," Opt. Lett. **31**, 1714–1716 (2006).
141. Y. Liu and H. K. Tsang, "Time dependent density of free carriers generated by two photon absorption in silicon waveguides," Appl. Phys. Lett. **90**, 211105 (2007).
142. M. Först, J. Niehusmann, T. Plötzing, J. Bolten, T. Wahlbrink, C. Moormann, and H. Kurz, "High-speed all-optical switching in ion-implanted silicon-on-insulator microring resonators," Opt. Lett. **32**, 2046–2048 (2007).
143. T. Tanabe, K. Nishiguchi, A. Shinya, E.Kuramochi, H. Inokawa, and M. Notomi, "Fast all-optical switching using ion-implanted silicon photonic crystal nanocavities," Appl. Phys. Lett. **90**, 031115 (2007).
144. D. Dimitropoulos, S. Fathpour, and B. Jalali, "Limitations of active carrier removal in silicon Raman amplifiers and lasers," Appl. Phys. Lett. **87**, 261108 (2005).
145. J. M. Ralston and R. K. Chang, "Spontaneous-Raman-scattering efficiency and stimulated scattering in silicon", Phys. Rev. B **2**, 1858 (1970).
146. J. B. Renucci, R. N. Tyte, and M. Cardona, "Resonant Raman scattering in silicon", Phys. Rev. B **11**, 3885 (1975).
147. T. A. Birks, W. J. Wadsworth, and P. St. J. Russell, "Supercontinuum generation in tapered fibers," Opt. Lett. **25**, 1415–1416 (2000).
148. P. St. J. Russell, "Photonic crystal fibers," IEEE J. Lightwave Technol. **24**, 4729–4749 (2006).
149. A. C. Turner, C. Manolatou, B. S. Schmidt, M. Lipson, M. A. Foster, J. E. Sharping, and A. L. Gaeta, "Tailored anomalous group-velocity dispersion in silicon channel waveguides," Opt. Express **14**, 4357–4362 (2006).
150. N. Bloembergen and P. Lallemand, "Complex intensity-dependent index of refraction, frequency broadening of stimulated Raman scattering, and stimulated Rayleigh scattering," Phys. Rev. Lett. **16**, 81–84 (1966).
151. K. Kikuchi, "Highly sensitive interferometric autocorrelator using Si avalanche photodiode as two-photon absorber," Electron. Lett. **34**, 123–125 (1998).
152. C. Xu, J. M. Roth, W. H. Knox, K. Bergman, "Ultra-sensitive autocorrelation of 1.5 μm light with single photon counting silicon avalanche photodiode," Electron. Lett. **38**, 86–88 (2002).
153. T. K. Liang, H. K. Tsang, T. E. Day, J. Drake, A. P. Knights, M. Asghari, "Silicon waveguide two-photon absorption detector at 1.5 μm wavelength for autocorrelation measurements," Appl. Phys. Lett. **81**, 1323–1325 (2002).
154. D. Panasenko, Y. Fainman, "Single-shot sonogram generation for femtosecond laser pulse diagnostics by use of two-photon absorption in a silicon CCD camera," Opt. Lett. **27**, 1475–1477 (2002).
155. R. Salem, G. E. Tudury, T. U. Horton, G. M. Carter, T. E. Murphy, "Polarization-insensitive optical clock recovery at 80 Gb/s using a silicon photodiode," IEEE Photon. Technol. Lett. **17**, 1968–1970 (2005).
156. M. Dinu, D. C. Kilper, H. R. Stuart, "Optical performance monitoring using data stream intensity autocorrelation," IEEE J. Lightwave Technol. **24**, 1194–1202 (2006).
157. K. Taira, Y. Fukuchi, R. Ohta, K. Katoh, and K. Kikuchi, "Background-free intensity autocorrelator employing Si avalanche photodiode as two-photon absorber," Electron. Lett. **38**, 1465-1466 (2002).
158. T. J. Kippenberg, S. M. Spillane, B. Min, and K. J. Vahala, "Theoretical and Experimental Study of Stimulated and Cascaded Raman Scattering in Ultrahigh-Q Optical Microcavities," IEEE J. Sel. Top. Quantum Electron. **10**, 1219–1228 (2004).
159. J. Hansryd, P. A. Andrekson, M. Westlund, J. Li, and P. Hedekvist, "Fiber-based optical parametric amplifiers and their applications," IEEE J. Sel. Top. Quantum Electron. **8**, 506–520 (2002).
160. S. Fathpour, K. K. Tsia, and B. Jalali, "Energy harvesting in silicon Raman amplifiers," Appl. Phys. Lett. **89**, 061109 (2006).
161. K. K. Tsia, S. Fathpour, and B. Jalali, "Energy harvesting in silicon wavelength converters," Opt. Express **14**, 12327–12333 (2006).
162. T. Torounidis and P. Andrekson, "Broadband single-pumped fiber-optic parametric amplifiers," IEEE Photon. Technol. Lett. **19**, 650–652 (2007).
163. J. M. Chavez Boggio, J. D. Marconi, S. R. Bickham, and H. L. Fragnito, "Spectrally flat and broadband dou-

#88416 - $15.00 USD Received 9 Oct 2007; revised 22 Nov 2007; accepted 25 Nov 2007; published 29 Nov 2007

blepumped fiber optical parametric amplifiers," Opt. Express **15**, 5288–5309 (2007).
164. M. D. Levenson, C. Flytzanis, and N. Bloembergen, "Interference of resonant and nonresonant three-wave mixing in diamond," Phys. Rev. B **6**, 3962–3965 (1972).
165. M. D. Levenson and S. Kano, *Intronduction to Nonlinear Laser Spectroscopy* (Academic Press, Boston, 1988).
166. B. Jalali, V. Raghunathan, R. Shori, S. Fathpour, D. Dimitropoulos, and O. Stafsudd, "Prospects for silicon Mid-IR Raman Lasers," IEEE J. Sel. Top. Quantum Electron. **12**, 1618–1627 (2006).
167. H. Takesue and K. Inoue, "Generation of polarization-entangled photon pairs and violation of Bell's inequality using spontaneous four-wave mixing in a fiber loop," Phys. Rev. A **70**, 031802(R) (2004).
168. X. Li, P. L. Voss, J. E. Sharping, and P. Kumar, "Optical-Fiber Source of Polarization-Entangled Photons in the 1550 nm Telecom Band," Phys. Rev. Lett. **94**, 053601 (2005).
169. J. Fulconis, O. Alibart, W. J. Wadsworth, P. St. J. Russell, and J. G. Rarity, "High brightness single mode source of correlated photon pairs using a photonic crystal fiber," Opt. Express **13**, 7572–7582 (2005).
170. J. Fan, A. Migdall, and L. J. Wang, "Efficient generation of correlated photon pairs in a microstructure fiber," Opt. Lett. **30**, 3368–3370 (2005).
171. X. Li, J. Chen, P. Voss, J. Sharping, and P. Kumar, "All-fiber photon-pair source for quantum communications: Improved generation of correlated photons," Opt. Express **12**, 3737–3744 (2004).
172. Q. Lin, F. Yaman, and G. P. Agrawal, "Photon-pair generation by four-wave mixing in optical fibers," Opt. Lett. **31**, 1286–1288 (2006).
173. Q. Lin, F. Yaman, and G. P. Agrawal, "Photon-pair generation in optical fibers through four-wave mixing: Role of Raman scattering and pump polarization," Phys. Rev. A **75**, 023803 (2007).
174. H. Takesue and K. Inoue, "1.5-μm band quantum-correlated photon pair generation in dispersion-shifted fibers: suppression of noise photons by cooling fiber," Opt. Express **13**, 7832–7839 (2005).
175. K. F. Lee, J. Chen, C. Liang, X. Li, P. L. Voss, and P. Kumar, "Generation of high-purity telecom-band entangled photon pairs in dispersion-shifted fiber," Opt. Lett. **31**, 1905–1907 (2006).

1. Introduction

Silicon photonics has attracted much attention recently because of its potential applications in the spectral region extending from near- to mid-infrared [1–3]. Silicon crystals, with a band gap near 1.12 eV, become nearly transparent in the spectral region beyond 1.1 μm and exhibit optical properties that are useful for a variety of applications [4]. The high refractive index of silicon allows for a tight confinement of optical waves to a sub-micron region using the silicon-on-insulator (SOI) technology [1]. Moreover, silicon exhibits a large third-order nonlinearity, with a Kerr coefficient more than 100 times larger [5] and a Raman gain coefficient more than 1000 times larger [6] than those of silica glass in the telecommunication band. These features enable efficient nonlinear interaction of optical waves at relatively low power levels inside a short SOI waveguide ($<$5 cm long). For this reason, considerable effort has been directed in recent years toward investigating the nonlinear phenomena such as self-phase modulation (SPM) [7–23], cross-phase modulation (XPM) [14, 24–26], stimulated Raman scattering (SRS) [27–60], and four-wave mixing (FWM) [61–79]. All of these nonlinear effects are currently being explored to realize a variety of optical functions on the chip scale.

Although the third-order nonlinear effects have been studied extensively for silica fibers [80], and these studies can be used as a guidance for SOI waveguides, it is important to remember that silicon is a semiconductor crystal exhibiting unique features such as two-photon absorption (TPA) [5, 7], free-carrier dispersion [81], and anisotropic and dispersive third-order nonlinearity [5, 82–87]. The interplay among various dispersive and nonlinear effects leads to many interesting features [8–25, 88, 89] that provide new functionalities on the one hand [90–100], but may become obstacles in some cases on the other [25, 32, 33, 35–37, 39, 65–68, 89]. Therefore, it is important to have a unified theoretical platform that not only can be used for understanding the underlying physics but also provides guidance toward new and useful applications. Indeed, considerable efforts have been made in the past few years to develop a theoretical approach for understanding a specific nonlinear phenomenon [13–16, 20–22, 26, 28, 46–48, 50, 55, 58, 59, 62, 66, 68, 70, 73, 74, 76, 88, 96]. In this paper, we review recent progress realized in modeling nonlinear phenomena inside SOI waveguides

#88416 - $15.00 USD Received 9 Oct 2007; revised 22 Nov 2007; accepted 25 Nov 2007; published 29 Nov 2007

and develop a unified theoretical platform. We then apply it to investigate various nonlinear effects occurring inside silicon waveguides with a keen eye toward their applications.

The paper is organized as follows. We begin in Section 2 with a description of the third-order nonlinearity of silicon and consider the tensorial nature of both the electronic and Raman contributions. The generation of free carriers through two-photon absorption and their impact on various nonlinear phenomena is included fully within the theory presented here. We derive a general propagation equation in the frequency domain and show how it leads to a generalized nonlinear Schrödinger equation when it is converted to the time domain. We use this equation in Section 3 to study propagation of ultrashort optical pulses in the presence of self-phase modulation and show the possibility of soliton formation and supercontinuum generation. The nonlinear phenomena of cross-phase modulation and stimulated Raman scattering are discussed in Section 4 with emphasis on the impact of free carriers on Raman amplification and lasing. Section 5 focuses on the FWM process and its applications. We consider first the impact of free carriers and show that, although index changes induced by them have a negligible impact on FWM, free-carrier absorption limits the FWM efficiency so much that a net positive gain is difficult to be realized with CW pumping in the telecommunication band. However, this problem can be solved by pumping at wavelengths beyond 2.2 μm because TPA-induced free carriers are then absent. We also show that FWM can occur over a wide bandwidth (>300 nm), with a proper choice of the pump wavelength, because of much smaller waveguide lengths employed compared with those required for silica fibers. We discuss briefly the use of FWM in silicon waveguides for generating correlated photon pairs that are useful for quantum applications.

2. General formalism

The nonlinear interactions of optical waves inside silica fibers are well understood owing to extensive investigations over the past few decades [80]. The so-called generalized nonlinear Schrödinger (NLS) equation provides a fairly accurate description, even for ultrashort pulses creating an octave-spanning supercontinuum [101]. As the origin of third-order nonlinearity in silicon waveguides is quite similar to that for silica fibers, a similar theoretical formalism can be used for silicon waveguides, with suitable modifications to account for the features unique to silicon. In this section, we develop a general formalism that can be used to describe various nonlinear effects inside silicon waveguides.

2.1. Third-order susceptibility of silicon

As silicon crystals exhibit an inversion symmetry, the lowest-order nonlinear effects stem from the third-order susceptibility $\chi^{(3)}$. When an optical field $\boldsymbol{E}(\boldsymbol{r},t)$ propagates inside a silicon crystal or waveguide, the induced nonlinear polarization can be written in the frequency domain in the general form [102, 103]

$$\widetilde{P}_i^{(3)}(\boldsymbol{r},\omega_i) = \frac{3\varepsilon_0}{4(2\pi)^2}\iint \chi_{ijkl}^{(3)}(-\omega_i;\omega_j,-\omega_k,\omega_l)\widetilde{E}_j(\boldsymbol{r},\omega_j)\widetilde{E}_k^*(\boldsymbol{r},\omega_k)\widetilde{E}_l(\boldsymbol{r},\omega_l)d\omega_j d\omega_k, \quad (1)$$

where $\omega_l \equiv \omega_i + \omega_k - \omega_j$, and we have adopted the notation of Ref. [102]. Here, i, j, k, and l take values x, y, and z and $\widetilde{E}_i(\boldsymbol{r},\omega)$ is the Fourier transform of the ith component $E_i(\boldsymbol{r},t)$ of the electric field defined as $\widetilde{B}(\boldsymbol{r},\omega) = \int_{-\infty}^{\infty} B(\boldsymbol{r},t)\exp(i\omega t)\,dt$. In Eq. (1), we have excluded the sum-frequency generation assuming that this process is not phase-matched.

The third-order susceptibility of silicon has two dominant contributions, one from bound electrons and the other from optical phonons, and it is useful to write it as $\chi_{ijkl}^{(3)} = \chi_{ijkl}^{e} + \chi_{ijkl}^{R}$, where the second term represents the Raman contribution involving optical phonons. These two terms have quite different dispersion and polarization characteristics.

#88416 - $15.00 USD Received 9 Oct 2007; revised 22 Nov 2007; accepted 25 Nov 2007; published 29 Nov 2007

Consider the Raman contribution first. Raman scattering in silicon is dominated by optical phonons near the Brillouin-zone center. As these phonons have three degenerate normal modes (with the same phonon energy), the Raman susceptibility is given by [104–106]

$$\chi^R_{ijkl}(-\omega_i;\omega_j,-\omega_k,\omega_l) = g'\widetilde{H}_R(\omega_l-\omega_k)\sum_{v=x,y,z}\mathscr{R}^v_{ij}\mathscr{R}^v_{kl} + g'\widetilde{H}_R(\omega_j-\omega_k)\sum_{v=x,y,z}\mathscr{R}^v_{il}\mathscr{R}^v_{jk}, \quad (2)$$

where the spectral response of Raman scattering, $\widetilde{H}_R(\Omega)$, is the same for three normal modes. Unlike silica glass which has a very broad Raman spectrum [107], optical phonons at the Brillouin-zone center of silicon have a well-defined frequency of $\Omega_R/2\pi = 15.6$ THz at room temperature [108–110], resulting in a relatively narrow Raman-gain spectrum, with a Lorentzian shape of the form [104–106]

$$\widetilde{H}_R(\Omega) = \frac{\Omega_R^2}{\Omega_R^2 - \Omega^2 - 2i\Gamma_R\Omega}. \quad (3)$$

Here Γ_R is related inversely to the phonon lifetime (about 3 ps), resulting in a full width at half-maximum (FWHM) of the Raman-gain spectrum of $\Gamma_R/\pi \approx 105$ GHz at room temperature [108]. In general, both Ω_R and Γ_R are sensitive to temperature [37, 108, 109]. As an example, $\Omega_R/2\pi$ decreases by ~40 GHz, while Γ_R/π increases by ~ 10 GHz, if temperature increases by 50°C. The parameter g' in Eq. (2) is related to the Raman polarizability associated with the Brillouin-zone-center phonons and is nearly independent of optical frequency [102, 104, 106]. It determines the peak value of the Raman gain coefficient that is discussed later in Section 2.4.

In Eq. (2), the Raman tensor $\mathscr{R}^v_{ij}$ describes polarization dependence of Raman scattering. As the three phonon modes belong to the $\Gamma_{25'}$ symmetry group and are polarized along a crystallographic axis (indicated by the superscript of $\mathscr{R}$), they interact resonantly only with optical waves polarized orthogonal to their own axes. For this reason, the three Raman tensors have the form [111]

$$\mathscr{R}^x_{ij} = \delta_{iy}\delta_{jz} + \delta_{iz}\delta_{jy}, \qquad \mathscr{R}^y_{ij} = \delta_{ix}\delta_{jz} + \delta_{iz}\delta_{jx}, \qquad \mathscr{R}^z_{ij} = \delta_{ix}\delta_{jy} + \delta_{iy}\delta_{jx}, \quad (4)$$

where we have assumed that x, y, and z axes are oriented along the crystallographic axes. Substituting Eq. (4) in Eq. (2), we obtain the following compact form for the Raman susceptibility:

$$\begin{aligned}\chi^R_{ijkl}(-\omega_i;\omega_j,-\omega_k,\omega_l) = {} & g'\widetilde{H}_R(\omega_l-\omega_k)(\delta_{ik}\delta_{jl} + \delta_{il}\delta_{jk} - 2\delta_{ijkl}) \\ & + g'\widetilde{H}_R(\omega_j-\omega_k)(\delta_{ik}\delta_{jl} + \delta_{ij}\delta_{kl} - 2\delta_{ijkl}), \end{aligned} \quad (5)$$

where δ_{ijkl} equals 1 only when $i = j = k = l$ and is 0 otherwise.

The Raman susceptibility in Eq. (5) describes Raman scattering involving a single phonon. Apart from this dominant contribution, Raman scattering can also involve multiple phonons simultaneously, a process known as higher-order Raman scattering [106, 108, 110]. In the case of silicon, the second-order Raman scattering exhibits a broadband peak at a frequency near 29 THz resulting from two transverse optical phonons and another peak around 9 THz associated with two transverse acoustic phonons. However, as their amplitudes are more than 50 and 200 times smaller, respectively, compared with the dominant first-order Raman peak [108, 110], higher-order Raman effects are negligible in most practical situations.

Optical waves can also interact with a single acoustic phonon and experience Brillouin scattering. However, the relative strength of this process in silicon is nearly two orders of magnitude smaller than that of first-order Raman scattering [112]. As a result, Brillouin scattering is negligible in most cases. This is in strong contrast to silica glass, where Brillouin scattering is three orders of magnitude stronger than Raman scattering [80]. In this paper, we neglect the effects of Brillouin scattering.

#88416 - $15.00 USD Received 9 Oct 2007; revised 22 Nov 2007; accepted 25 Nov 2007; published 29 Nov 2007

We next focus on the electronic contribution stemming from oscillations of bound electrons and leading to the optical Kerr effect through intensity-dependent changes in the refractive index. It also leads to two-photon absorption (TPA) whenever the energy of photons exceeds the half band gap $E_g/2$, where $E_g \approx 1.12$ eV for silicon corresponds to a wavelength of 1.1 μm. Bound electrons in the valence band can be excited to the conduction band through TPA by absorbing two photons with total energy exceeding E_g. This process has to be assisted by phonons to conserve momentum because of the indirect nature of the band gap in silicon [113,114]. The response time of both the Kerr effect and the TPA process are extremely short. As an estimate, the uncertainty principle implies that non-resonant electronic transition occurs on a time scale of $|\omega - E_g/\hbar|^{-1}$. For frequencies well below the band gap, the response time is below 10 fs [102, 115]. Such a nearly instantaneous nature of electronic nonlinear response leads to many potential applications related to high-speed optical signal processing [116].

Equation (1) shows that a complete description of third-order nonlinear effects requires knowledge of the tensorial and dispersive properties of $\chi^e_{ijkl}(-\omega_i;\omega_j,-\omega_k,\omega_l)$. Fortunately, as a silicon crystal belongs to the *m*3*m* point-group symmetry, its electronic nonlinear response has only four independent components [103, 117, 118]:

$$\chi^e_{ijkl} = \chi^e_{1122}\delta_{ij}\delta_{kl} + \chi^e_{1212}\delta_{ik}\delta_{jl} + \chi^e_{1221}\delta_{il}\delta_{jk} + \chi^e_d\delta_{ijkl}, \tag{6}$$

where $\chi^e_d \equiv \chi^e_{1111} - \chi^e_{1122} - \chi^e_{1212} - \chi^e_{1221}$ represents the nonlinearity anisotropy. In practice, the most relevant electronic nonlinearity is the one involving only one frequency, i.e., $\chi^e_{ijkl}(-\omega;\omega,-\omega,\omega)$. In this case, Eq. (6) is simplified considerably owing to the intrinsic permutation symmetry of $\chi^e_{1122}(-\omega;\omega,-\omega,\omega) = \chi^e_{1221}(-\omega;\omega,-\omega,\omega)$. Moreover, for photon energies $\hbar\omega$ well below E_g, $\chi^e_{1212}(-\omega;\omega,-\omega,\omega) \approx \chi^e_{1122}(-\omega;\omega,-\omega,\omega)$ [105, 118–121]. As a result, Eq. (6) reduces to

$$\chi^e_{ijkl} = \chi^e_{1111}\left[\frac{\rho}{3}\left(\delta_{ij}\delta_{kl} + \delta_{ik}\delta_{jl} + \delta_{il}\delta_{jk}\right) + (1-\rho)\delta_{ijkl}\right], \tag{7}$$

where $\rho \equiv 3\chi^e_{1122}/\chi^e_{1111}$ characterizes the nonlinear anisotropy at the degenerate frequency ω. Note that Eq. (7) remains valid for third harmonic generation [86, 118, 119, 122–125]. Also note that the value of ρ can be complex in general.

To characterize the electronic nonlinearity, one needs to measure $\chi^e_{1111}(-\omega;\omega,-\omega,\omega)$. The real and imaginary parts are related to the Kerr coefficient n_2 and the TPA coefficient β_T as [80, 102]

$$\frac{\omega}{c}n_2(\omega) + \frac{i}{2}\beta_T(\omega) = \frac{3\omega}{4\varepsilon_0 c^2 n_0^2(\omega)}\chi^e_{1111}(-\omega;\omega,-\omega,\omega), \tag{8}$$

where $n_0(\omega)$ is the linear refractive index of silicon at the frequency ω. Extensive measurements have been carried out to characterize n_2 and β_T over a wide frequency range [5–7, 9, 11, 12, 24, 65, 82–85, 93, 126]. The value of n_2 for silicon is found to be more than 100 times larger in the 1.55-μm region than that of fused silica. However, TPA is also quite large in this spectral region. The relative magnitudes of the Kerr and TPA coefficients are often characterized by a nonlinear figure of merit (NFOM) [127] defined as $F_n = n_2/(\lambda\beta_T)$, where $\lambda \equiv 2\pi c/\omega$ is the optical wavelength in vacuum. This NFOM is quite small for silicon (only about 0.3) in the 1.55-μm spectral region [5, 84]. Recent experiments [5, 82–85] show that n_2 and β_T also vary considerably with λ in the spectral region extending from 1.1 μm to 2.2 μm (close to half band gap), with n_2 peaking around 1.8-1.9 μm. Since TPA decreases quickly to zero when the wavelength exceeds 1.7 μm, the NFOM increases considerably for λ near or beyond 2 μm [84]. Unlike a direct band-gap semiconductor for which n_2 changes its sign at photon energies around $0.7E_g$ [128], n_2 for silicon is always positive for all photon energies below E_g [83, 84]. This is a consequence of the phonon-assisted nature of electronic nonlinearity [113, 114].

#88416 - $15.00 USD Received 9 Oct 2007; revised 22 Nov 2007; accepted 25 Nov 2007; published 29 Nov 2007

The magnitude of nonlinear anisotropy is related to the band structure of a silicon crystal. It has been measured in the past four decades through third-harmonic generation [86, 122–125], degenerate FWM [120, 121], and the z-scan technique [87]. The magnitude of ρ is quite dispersive in the opaque region ($\hbar\omega > E_g$) [86], but it becomes nearly constant for $\hbar\omega < E_g$ [86, 87, 120]. The measured value of ρ is close to 1.27 in the telecom band, with a negligible imaginary part [87]. The absence of an imaginary part indicates that anisotropy is the same for both the Kerr and TPA coefficients. From the standpoint of applications, nonlinear anisotropy affects the polarization dependence of nonlinear phenomena inside silicon waveguides. Recently, photocurrent induced by TPA inside a silicon avalanche photodiode (APD) was used to characterize the anisotropy of TPA [129, 130]. In contrast to the optical characterization, TPA-induced photocurrents indicated that the TPA process was isotropic inside a silicon APD. This discrepancy between the optical and electrical measurements remains an open issue at this time. One possible reason may be related to the nonlinear Franz–Keldysh effect [114] introduced by the high dc field inside an APD.

2.2. Free-carrier effects

The TPA process may generate a considerable number of free electrons and holes, depending on the peak power associated with the incident optical field. These excessive carriers not only absorb light but also affect the nature of wave propagation by changing the refractive index. As the electron and hole mobilities, μ_e and μ_h, in silicon are in the range of 100–1000 $\mathrm{cm}^2/(\mathrm{V}\cdot\mathrm{s})$ for densities of up to 10^{18} cm^{-3} [131], the momentum relaxation times [$\tau_v = \mu_v m_v^*/q$ ($v = e, h$), where m_v^* is the effective mass and q is electron's charge] lies in subpicosecond regime, much longer than the duration of an optical cycle [102]. As a result, free carriers can follow oscillations of an optical wave almost instantaneously and affect its propagation right after their creation. The dynamics of free carriers are well described by the Drude model [81, 102, 132–134], and the induced polarization varies linearly with the carrier densities as

$$P_i^{\mathrm{f}}(\boldsymbol{r},t) = N_e(\boldsymbol{r},t)\langle p_i^{\mathrm{e}}(\boldsymbol{r},t)\rangle + N_h(\boldsymbol{r},t)\langle p_i^{\mathrm{h}}(\boldsymbol{r},t)\rangle, \tag{9}$$

where N_e and N_h are densities of free electrons and holes, respectively. In this equation, $\langle p_i^{\,v}\rangle$ with $v = e, h$ is the statistically averaged response of a single electron or hole to the electric field. According to the Drude model, it takes a simple form in the frequency domain, $\langle \widetilde{p}_i^{\,\mathrm{v}}(\boldsymbol{r},\omega)\rangle = \varepsilon_0 \Upsilon_v(\omega)\widetilde{E}_i(\boldsymbol{r},\omega)$, where the carrier polarizability Υ_v is given by [102]

$$\Upsilon_v(\omega) = \frac{q^2\tau_v}{\varepsilon_0 m_v^*}\left(\frac{-1}{\omega(\omega\tau_v + i)}\right). \tag{10}$$

The carrier-induced polarization in the frequency domain is thus given by

$$\widetilde{P}_i^{\mathrm{f}}(\boldsymbol{r},\omega) = \varepsilon_0 \int \widetilde{\chi}^{\mathrm{f}}(\omega,\omega',\widetilde{N}_e,\widetilde{N}_h)\widetilde{E}_i(\boldsymbol{r},\omega')\,d\omega', \tag{11}$$

where the spectral response $\widetilde{\chi}^{\mathrm{f}}$ is defined as

$$\widetilde{\chi}^{\mathrm{f}}(\omega,\omega',\widetilde{N}_e,\widetilde{N}_h) \equiv \Upsilon_e(\omega')\widetilde{N}_e(\boldsymbol{r},\omega-\omega') + \Upsilon_h(\omega')\widetilde{N}_h(\boldsymbol{r},\omega-\omega'). \tag{12}$$

Here $\widetilde{N}_v$ ($v = e, h$) is the Fourier transform of the carrier density N_v. Equation (11) shows that the free-carrier response has a linear and isotropic nature, because of the cubic rotational symmetry of a silicon crystal [102].

Equation (10) indicates how the spectral response of free carriers varies with optical frequency. However, in most cases of nonlinear interactions, the optical field consists of only a

#88416 - $15.00 USD Received 9 Oct 2007; revised 22 Nov 2007; accepted 25 Nov 2007; published 29 Nov 2007

few waves at specific carrier frequencies ω_u, each of which has a limited bandwidth. On the other hand, carrier densities vary on a time scale longer than that associated with an optical pulse, *i.e.*, they vary much slower than the carrier dipole moment oscillating at optical frequencies. As a result, the time-domain induced polarization consists of a few terms, each of which adiabatically follows variations of carrier densities, while oscillating around a specific carrier frequency ω_u. More specifically,

$$P_i^{\mathrm{f}}(\boldsymbol{r},t) = \varepsilon_0 \sum_u \chi^{\mathrm{f}}(\omega_u, N_e, N_h) E_i(\boldsymbol{r},\omega_u,t), \tag{13}$$

where $E_i(\boldsymbol{r},\omega_u,t)$ is the optical field at the carrier frequency ω_u and the induced susceptibility is given by

$$\chi^{\mathrm{f}}(\omega_u, N_e, N_h) = \Upsilon_e(\omega_u) N_e(\boldsymbol{r},t) + \Upsilon_h(\omega_u) N_h(\boldsymbol{r},t). \tag{14}$$

As the susceptibility χ^{f} is complex in general [see Eq. (10)], we can relate its real and imaginary parts to changes in the refractive index and the absorption coefficient induced by free carriers using the relation,

$$\chi^{\mathrm{f}} = 2n_0[n_{\mathrm{f}} + ic\alpha_{\mathrm{f}}/(2\omega)], \tag{15}$$

where n_{f} is the free-carrier index (FCI) change and α_{f} governs free-carrier absorption (FCA). Ideally, according to the Drude model of Eq. (10), they vary with optical frequency as ($\omega\tau_v \gg 1$) [81, 102, 134]

$$n_{\mathrm{f}}(\omega, N_e, N_h) = -\frac{q^2}{2\varepsilon_0 n_0 \omega^2}\left(\frac{N_e}{m_e^*} + \frac{N_h}{m_h^*}\right), \tag{16}$$

$$\alpha_{\mathrm{f}}(\omega, N_e, N_h) = \frac{q^3}{\varepsilon_0 c n_0 \omega^2}\left(\frac{N_e}{\mu_e m_e^{*2}} + \frac{N_h}{\mu_h m_h^{*2}}\right). \tag{17}$$

In practice, their magnitudes for silicon are larger than those predicted by Eqs. (16) and (17). At a specific wavelength of $\lambda_r = 2\pi c/\omega_r = 1550$ nm, it is common to employ the following empirical formulas [81, 135]

$$n_{\mathrm{f}}(\omega_r, N_e, N_h) = -(8.8\times 10^{-4} N_e + 8.5 N_h^{0.8})\times 10^{-18}, \tag{18}$$

$$\alpha_{\mathrm{f}}(\omega_r, N_e, N_h) = (8.5 N_e + 6.0 N_h)\times 10^{-18}, \tag{19}$$

where N_e and N_h have units of cm^{-3} and α_{f} is expressed in units of cm^{-1}.

In the case of nonlinear optical interactions, free carriers are created through TPA with equal densities, i.e., $N_e = N_h \equiv N$. In this case, it is more convenient to write n_{f} and α_{f} as

$$n_{\mathrm{f}} = \sigma_n(\omega) N, \qquad \alpha_{\mathrm{f}} = \sigma_a(\omega) N, \tag{20}$$

where $\sigma_a = 1.45\times 10^{-17}(\omega_r/\omega)^2$ (in units of cm^2) and $\sigma_n = \varsigma(\omega_r/\omega)^2$. The value of ς depends on the density region because of the $(N_h)^{0.8}$ dependence for holes in Eq. (18). For example, Eq. (18) shows that the contribution of holes is about 3.8 and 6.1 times larger than that of electrons for a density of 10^{17} and 10^{16} cm^{-3}, respectively. As the carrier density created by TPA is typically in this range, we assume that the hole contribution to FCI is 5 times that of electrons, and use $\varsigma \approx -5.3\times 10^{-21}$ (in units of cm^3) in this paper.

Equations (16), (17), and (20) show that FCI and FCA changes with time reflect precisely temporal variations of free carriers. This feature has been widely used to investigate the carrier dynamics in semiconductors by probing the transient FCI and FCA excited by an ultrashort pump pulse [132, 133]. Note that the model presented in this section for free-carrier effects is valid only when free carriers reach a certain thermal quasi-equilibrium. This is the case for

#88416 - $15.00 USD Received 9 Oct 2007; revised 22 Nov 2007; accepted 25 Nov 2007; published 29 Nov 2007

time scales >50 fs because optically excited free carriers can be thermalized over such time intervals by various scattering processes [132, 133, 136]. In the context of nonlinear silicon photonics, almost all practical applications fall in this regime. However, a quantum-mechanical description is necessary for accurate modeling of free-carrier dynamics for ultrashort pulses containing only of a few optical cycles [136].

Apart from density changes, optical excitation of free carriers between nonparabolic conduction and valence bands may also modify the effective masses of electrons and holes and thus introduce additional nonlinear effects associated with free carriers [134]. However, this effect is minor compared with the changes in the carrier density and is neglected in this paper.

2.3. General frequency-domain wave equation

In this subsection we derive a general equation describing propagation of an optical field inside a silicon waveguide. As usual, the starting point is the Maxwell wave equation. After including the induced polarizations associated with the third-order nonlinearity and free carriers, the wave equation in the frequency domain takes the form

$$\nabla^2 \widetilde{E}_i(\boldsymbol{r},\omega) + \frac{\omega^2}{c^2} n_0^2(\omega) \widetilde{E}_i(\boldsymbol{r},\omega) = -\mu_0 \omega^2 \left[\widetilde{P}_i^{\mathrm{f}}(\boldsymbol{r},\omega) + \widetilde{P}_i^{(3)}(\boldsymbol{r},\omega) \right]. \tag{21}$$

In general, the induced polarizations are only small perturbations to the linear wave equation. To the first order, we can assume that the waveguide modes are not affected by them and write the electric field in the form

$$\widetilde{E}_i(\boldsymbol{r},\omega) \approx \widetilde{F}_i(x,y,\omega) \widetilde{A}_i(z,\omega), \tag{22}$$

where $\widetilde{F}_i(x,y,\omega)$ governs the mode profile in the plane transverse to the propagation direction z. Substituting Eq. (22) into Eq. (21), multiplying by $\widetilde{F}_i^*$, and integrating over the transverse plane, we obtain

$$\frac{\partial^2 \widetilde{A}_i}{\partial z^2} + \beta_i^2(\omega) \widetilde{A}_i = -\mu_0 \omega^2 \frac{\iint \widetilde{F}_i^* [\widetilde{P}_i^{\mathrm{f}} + \widetilde{P}_i^{(3)}] \, dxdy}{\iint |\widetilde{F}_i|^2 dxdy}, \tag{23}$$

where $\beta_i(\omega)$ is the propagation constant given by

$$\beta_i^2(\omega) = \frac{\omega^2}{c^2} \frac{\iint n_0^2(\omega) |\widetilde{F}_i|^2 dxdy}{\iint |\widetilde{F}_i|^2 dxdy} + \frac{\iint \widetilde{F}_i^* \nabla_T^2 \widetilde{F}_i \, dxdy}{\iint |\widetilde{F}_i|^2 dxdy}, \tag{24}$$

and the subscript T denotes the transverse part of the Laplacian operator. The linear dispersion curve of a silicon waveguide is obtained from Eq. (24) after finding the transverse mode profile under specific boundary conditions set by the waveguide geometry. Note that the material refractive index n_0 is generally different for the core and cladding layers.

The general solution of Eq. (23), in the absence of the free-carrier and nonlinear effects, consists of the forward and backward propagating waves with the phase factors $e^{\pm i\beta_i(\omega)z}$. This phase factor varies in a length scale of optical wavelength, much shorter than the length scale in which the small free-carrier and third-order nonlinear effects evolve. As a result, $\partial \widetilde{A}_i / \partial z \approx i\beta_i(\omega)\widetilde{A}_i$ even when the free-carrier and nonlinear effects are included, where we have assumed that the incident optical field propagates along the $+z$ direction. Assuming that small perturbations do not reflect light and the backward wave can thus be ignored, we make the slowly varying envelope approximation and use

$$\frac{\partial^2}{\partial z^2} + \beta_i^2 = \left(\frac{\partial}{\partial z} + i\beta_i \right) \left(\frac{\partial}{\partial z} - i\beta_i \right) \approx 2i\beta_i \left(\frac{\partial}{\partial z} - i\beta_i \right). \tag{25}$$

#88416 - $15.00 USD Received 9 Oct 2007; revised 22 Nov 2007; accepted 25 Nov 2007; published 29 Nov 2007

As a result, Eq. (23) reduces to

$$\frac{\partial \widetilde{A}_i}{\partial z} = i\beta_i(\omega)\widetilde{A}_i + \frac{i\mu_0\omega^2}{2\beta_i(\omega)} \frac{\iint \widetilde{F}_i^*[\widetilde{P}_i^{\mathrm{f}} + \widetilde{P}_i^{(3)}]\,dxdy}{\iint |\widetilde{F}_i|^2\,dxdy}. \tag{26}$$

By substituting Eq. (22) into Eqs. (1) and (11) and using them in Eq. (26), we obtain the following equation for the field amplitude:

$$\begin{aligned}\frac{\partial \widetilde{A}_i}{\partial z} &= i\beta_i(\omega)\widetilde{A}_i + i\int \widetilde{\beta}_i^{\mathrm{f}}(\omega,\omega',\widetilde{N}_e,\widetilde{N}_h)\widetilde{A}_i(z,\omega')\,d\omega' \\ &\quad + \frac{i}{4\pi^2}\iint \gamma_{ijkl}(-\omega;\omega_j,-\omega_k,\omega_l)A_j(z,\omega_j)A_k^*(z,\omega_k)A_l(z,\omega_l)\,d\omega_j d\omega_k,\end{aligned} \tag{27}$$

where we have normalized the field amplitude such that the corresponding temporal profile $|A(z,t)|^2$ has units of power. The nonlinear parameter γ_{ijkl} in Eq. (27) is defined as

$$\gamma_{ijkl}(-\omega_i;\omega_j,-\omega_k,\omega_l) = \frac{3\omega_i\eta_{ijkl}}{4\varepsilon_0 c^2\overline{a}(n_i n_j n_k n_l)^{1/2}}\chi^{(3)}_{ijkl}(-\omega_i;\omega_j,-\omega_k,\omega_l), \tag{28}$$

where $n_v(\omega_v) = c\beta_v(\omega_v)/\omega_v$ ($v = i,j,k,l$) is the modal refractive index at ω_v, $\overline{a}$ is the *average* effective mode area related to that at individual frequencies as

$$\overline{a} \equiv (a_i a_j a_k a_l)^{1/4}, \qquad a_v = \frac{[\iint |\widetilde{F}_v|^2 dxdy]^2}{\iint |\widetilde{F}_v|^4 dxdy}, \tag{29}$$

and η_{ijkl} is the mode-overlap factor defined as

$$\eta_{ijkl} \equiv \frac{\iint \widetilde{F}_i^*\widetilde{F}_j\widetilde{F}_k^*\widetilde{F}_l\,dxdy}{\left[\prod_{v=i,j,k,l}\iint |\widetilde{F}_v|^4\,dxdy\right]^{1/4}}. \tag{30}$$

The integral in the numerator of a_v is over the whole transverse plane, but the dominant contribution to other integrals in Eqs. (29) and (30) comes from the silicon core layer if the third-order susceptibility is negligible for cladding layers.

Similar to $\chi^{(3)}_{ijkl}$, the nonlinear parameter $\gamma_{ijkl} = \gamma^e_{ijkl} + \gamma^R_{ijkl}$ is also composed of the electronic and Raman parts. Its expression in Eq. (28) includes wavelength dependence of the nonlinear parameters, effective mode area, mode overlap, and modal refractive index. If only one wave at the frequency ω_i is involved, $\eta_{iiii} = 1$, $\overline{a} = a_i$, and Eq. (28) reduces to the conventional nonlinear parameter [80]. A detailed analysis shows that the fundamental modes of a straight waveguide overlap well with each other, leading to $\eta_{ijkl} \approx 1$. But this is not so for a microdisk or microring resonator because of the curved nature of device geometry [137].

In Eq. (27), the second term on the right side represents the effect of free carriers with $\widetilde{\beta}_i^{\mathrm{f}}$ given by

$$\widetilde{\beta}_i^{\mathrm{f}}(\omega,\omega',\widetilde{N}_e,\widetilde{N}_h) = \frac{\omega}{2cn_i(\omega)}\frac{\iint \widetilde{\chi}^{\mathrm{f}}(\omega,\omega',\widetilde{N}_e,\widetilde{N}_h)|\widetilde{F}_i|^2\,dxdy}{\iint |\widetilde{F}_i|^2\,dxdy}, \tag{31}$$

where $\widetilde{\chi}^{\mathrm{f}}$ is given in Eq. (12). In general, free carriers have specific transverse density distributions inside the waveguide, and $\widetilde{\beta}_i^{\mathrm{f}}$ includes the effect of a partial overlap between the charge distribution and the mode profile [138]. If we assume that $\widetilde{\chi}^{\mathrm{f}}$ is linearly proportional to the carrier densities [see Eqs. (9) through (20)], Eq. (31) is simplified, resulting in the following expression:

$$\widetilde{\beta}_i^{\mathrm{f}} = \frac{\omega}{2cn_i(\omega)}\widetilde{\chi}^{\mathrm{f}}(\omega,\omega',\widetilde{\overline{N}}_e,\widetilde{\overline{N}}_h), \qquad \widetilde{\overline{N}}_v = \frac{\iint \widetilde{N}_v|\widetilde{F}_i|^2 dxdy}{\iint |\widetilde{F}_i|^2 dxdy}. \tag{32}$$

#88416 - $15.00 USD Received 9 Oct 2007; revised 22 Nov 2007; accepted 25 Nov 2007; published 29 Nov 2007

The physical meaning of free-carrier effects can be seen more clearly in the time domain. The general form of the free-carrier term in Eq. (27) can be simplified considerably if we notice that nonlinear interactions typically involve only a few optical waves, each with a limited bandwidth around a carrier frequency ω_u. By using Eqs. (13) and (14), it is easily to show that the free-carrier effects on each wave manifest in the time domain as a perturbation to the propagation constant through FCI and FCA. From Eqs. (13), (15), and (32), this perturbation is given by

$$\beta_i^{\mathrm{f}}(\omega_u, \bar{N}_e, \bar{N}_h) = \frac{n_0(\omega_u)}{n_i(\omega_u)} \left[\frac{\omega_u}{c} n_{\mathrm{f}}(\omega_u, \bar{N}_e, \bar{N}_h) + \frac{i}{2} \alpha_{\mathrm{f}}(\omega_u, \bar{N}_e, \bar{N}_h) \right], \tag{33}$$

where n_{f} and α_{f} are given by Eqs. (16) and (17) [or Eqs. (18)–(20)] after replacing N_e and N_h with their averaged values defined in Eq. (32). Equation (33) shows that, for the same distribution of carrier densities, free-carrier effects are enhanced in a waveguide compared with bulk material as the modal refractive index is smaller because of mode confinement. The free carriers may also introduce extra birefringence or polarization-dependent losses because n_i can be quite different for different polarization modes. Such effects are negligible for waveguides with a relatively large mode area, but they can become significant inside a nano-size waveguide. As an example, for an air-clad SOI waveguide with a cross section of $600 \times 300\ \mathrm{nm}^2$, n_i is 2.76 and 2.32 at $\lambda = 1.55\ \mu$m for the fundamental TE and TM modes, respectively. These values are much smaller than the material index ($n_0 = 3.48$) and indicate that free-carrier effects would be enhanced by 26 and 50% for the TE and TM modes, respectively.

Free electrons and holes can be generated either optically inside the waveguide or electrically through current injection from outside. After being created, they can diffuse to a low-density area through thermal motion, or drift away by an external dc electric field $\boldsymbol{E}_{\mathrm{dc}}$. In general, the dynamics of carrier density is governed by the continuity equation [131]

$$\frac{\partial N_v}{\partial t} = G - \frac{N_v}{\tau_v'} + D_v \nabla^2 N_v - s_v \mu_v \boldsymbol{\nabla} \cdot (N_v \boldsymbol{E}_{\mathrm{dc}}), \tag{34}$$

where $v = e$ for electrons, $v = h$ for holes, $s_h = 1$, $s_e = -1$, D_v is the diffusion coefficient, τ_v' is the carrier lifetime, and μ_v is the mobility. The generation rate G is a function of optical field, if free carriers are generated through optical excitation like TPA.

What we are interested in is not a detailed density distribution across the waveguide but its effect on the optical field. Thus, we can average Eq. (34) over the transverse coordinates to obtain a dynamic equation for the average density $\bar{N}_v$. By noting that the diffusion and drift of carriers away from the waveguide core reduces carrier density inside it, just as recombination of carriers does, we write the spatially averaged terms in Eq. (34) as

$$\frac{\iint |\widetilde{F}_i|^2 \left[D_v \nabla^2 N_v - s_v \mu_v \boldsymbol{\nabla} \cdot (N_v \boldsymbol{E}_{\mathrm{dc}}) \right] dxdy}{\iint |\widetilde{F}_i|^2 dxdy} = -\frac{\bar{N}_v}{\tau_v^*}, \tag{35}$$

where τ_v^* represents the effective lifetime associated with thermal diffusion and field-induced drift of free carriers. As a result, the dynamics of averaged carrier densities are governed by a simple equation of the form

$$\frac{\partial \bar{N}_v}{\partial t} = \bar{G} - \frac{\bar{N}_v}{\tau_0}, \qquad \bar{G} = \frac{\iint G |\widetilde{F}_i|^2 dxdy}{\iint |\widetilde{F}_i|^2 dxdy}, \tag{36}$$

where $\bar{G}$ is the generation rate averaged over the optical mode profile and $\tau_0 \equiv \tau_v' \tau_v^* / (\tau_v' + \tau_v^*)$ is an effective carrier lifetime that includes all the effects of recombination, diffusion, and drift; we have assumed it to be the same for electrons and holes.

#88416 - $15.00 USD Received 9 Oct 2007; revised 22 Nov 2007; accepted 25 Nov 2007; published 29 Nov 2007

Note from Eq. (35) that the effective lifetime in general depends on the waveguide geometry. Indeed, it can be reduced considerably by increasing the surface-to-volume ratio of the waveguide [139]. It can also be reduced by applying an external dc field [42, 67] or introducing non-radiative centers through ion implantation [140–143]. However, as nonlinear interactions require relatively high intensity inside the waveguide, generated carriers may screen the applied dc field and thus limit the reduction in effective carrier lifetime [144]. For SOI waveguides commonly used for photonic applications, the effective lifetime varies from subnanosecond [54, 90, 141] to tens of nanoseconds [41, 42].

Equation (27) is quite general as it includes all dispersive, nonlinear, and polarization effects introduced by waveguide confinement, free carriers and third-order nonlinearity. The first term on its right side governs the dispersive effects. It can also include linear absorptive and scattering losses, if $\beta(\omega)$ is treated as a complex quantity. This frequency-domain wave equation can be used to investigate nonlinear interactions inside silicon waveguides for optical fields with arbitrary spectra. It can be simplified considerably if we notice that both the free-carrier and the third-order electronic nonlinear effects are only weakly dependent on optical frequency across a pulse spectrum. Often, the dispersion induced by FCI is negligible compared with the material and waveguide dispersion because $|n_{\rm f}| < 10^{-3}$ even at carrier densities up to 10^{17}cm^{-3} [81]. As $\alpha_{\rm f} \propto 1/\omega^2 \propto \lambda^2$ [see Eqs. (16) and (17)], the magnitude of FCA changes by <14% even when the wavelength changes over 100 nm in the 1.55-μm spectral band. For similar changes in the wavelength, the electronic nonlinearity of silicon varies by ~20% in this spectral region [83–85]. Thus, if the incident and generated optical fields have a bandwidth much smaller than 100 nm, we can employ the approximation $\gamma^e_{ijkl}(-\omega_i;\omega_j,-\omega_k,\omega_l) \approx \gamma^e_{ijkl}(-\omega_i;\omega_i,-\omega_i,\omega_i)$ and use Eq. (7). The use of this approximation simplifies the theory considerably.

2.4. Time-domain description

In many practical situations, the input field is either a continuous wave (CW) or is in the form of a pulse train. If only one wave at the carrier frequency ω_0 propagates along the waveguide, we can expand the propagation constant $\beta(\omega)$ in a Taylor series around ω_0. The time-domain description of the nonlinear process is then realized by replacing $\omega-\omega_0$ with the derivative $i(\partial/\partial t)$. Transferring Eq. (27) into time domain with this approach, we obtain the following equation for the field amplitude $A_i(z,t)$:

$$\frac{\partial A_i}{\partial z} = \sum_{m=0}^{\infty} \frac{i^{m+1}\beta_{im}}{m!}\frac{\partial^m A_i}{\partial t^m} + i\beta_i^{\rm f}(\omega_0,\bar{N}_e,\bar{N}_h)A_i + i\left(1+i\xi\frac{\partial}{\partial t}\right)P_i^{NL}, \tag{37}$$

where β_{im} is the mth-order dispersion parameter defined as $\beta_{im} = (d^m\beta_i/d\omega^m)|_{\omega=\omega_0}$. These parameters also include the linear loss and its dispersion when $\beta(\omega)$ is a complex quantity. In the following discussion, we assume that free carriers are generated only optically so that $\bar{N}_e = \bar{N}_h = \bar{N}$, and write the $\beta_i^{\rm f}$ term as $\beta_i^{\rm f}(\omega_0,\bar{N})$.

The nonlinear polarization $P_i^{NL}(z,t)$ has the following compact form in the time domain:

$$P_i^{NL}(z,t) = A_j(z,t)\int_{-\infty}^{\infty} R^{(3)}_{ijkl}(t-\tau)A_k^*(z,\tau)A_l(z,\tau)d\tau, \tag{38}$$

where the third-order nonlinear response function is given by

$$\begin{aligned} R^{(3)}_{ijkl}(\tau) = {} & \gamma_e(\omega_0)\delta(\tau)\left[\frac{\rho}{3}\left(\delta_{ij}\delta_{kl}+\delta_{ik}\delta_{jl}+\delta_{il}\delta_{jk}\right)+(1-\rho)\delta_{ijkl}\right] \\ & + \gamma_R h_R(\tau)\left(\delta_{ik}\delta_{jl}+\delta_{il}\delta_{jk}-2\delta_{ijkl}\right), \end{aligned} \tag{39}$$

The electronic nonlinear parameter $\gamma_e(\omega_0)$ is defined as

$$\gamma_e(\omega_0) \equiv \gamma^e_{1111}(-\omega_0;\omega_0,-\omega_0,\omega_0) \equiv \gamma_0(\omega_0) + \frac{i}{2}\beta_T'(\omega_0), \tag{40}$$

#88416 - $15.00 USD Received 9 Oct 2007; revised 22 Nov 2007; accepted 25 Nov 2007; published 29 Nov 2007

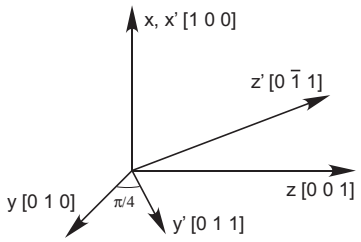

Fig. 1. Rotation of the coordinate system required for SOI waveguides fabricated along the $[0\ \bar{1}\ 1]$ direction.

where $\gamma_0 = \omega_0 n_2/(c\bar{a})$ is the nonlinear Kerr parameter and $\beta_T' = \beta_T/\bar{a}$ is the TPA coefficient normalized by the effective mode area.

The Raman nonlinear parameter γ_R is related to the Raman gain coefficient g_R as $\gamma_R(\omega_0) = g_R(\omega_0)\Gamma_R/(\bar{a}\Omega_R)$, where g_R is obtained from Eqs. (3) and (28) and is given by $g_R(\omega_0) = 3\omega_0 g'\Omega_R/(2\varepsilon_0 c^2 n^2 \Gamma_R)$. Note that g_R is linearly proportional to ω_0. In the 1.55-μm spectral band, its values are in the range of 4.3 to 76 cm/GW, based on the experimental measurements of spontaneous and stimulated Raman scattering [6, 27, 29, 30, 32, 34, 41, 145, 146]. Thus, g_R is more than 1000 times larger than that found for silica [80]. It is also nearly 10 times larger than the electronic nonlinear parameter of silicon. However, as γ_R depends linearly on Γ_R/Ω_R, the magnitude of γ_R is only a few percent of γ_0 and is negligible unless the pulse spectrum falls within the Raman gain bandwidth. The Raman response function $h_R(\tau)$ in Eq. (39) is the inverse Fourier transform of $\widetilde{H}_R(\Omega)$. Using Eq. (3), it is found to be [$h_R(t) = 0$ for $t < 0$]

$$h_R(t) = \Omega_R^2 \tau_1 e^{-t/\tau_2} \sin(t/\tau_1), \tag{41}$$

where $\tau_2 = 1/\Gamma_R$ and $\tau_1 = 1/(\Omega_R^2 - \Gamma_R^2)^{1/2} \approx 1/\Omega_R$. The Raman-gain bandwidth of 105 GHz in silicon corresponds to a response time of $\tau_2 \approx 3$ ps. Similarly, the Raman shift of 15.6 THz corresponds to $\tau_1 \approx 10$ fs.

Although Eq. (39) shows that the third-order nonlinearity involves all three components of the electric field, the longitudinal field component E_z in a silicon waveguide contains only a relatively small fraction of incident power, particularly in the case of the fundamental TE and TM modes. As a result, the nonlinear effects are dominated by the transverse polarization components of the electric field. For this reason, most problems can be simplified by neglecting the E_z component, as far as the nonlinear effects are concerned.

As discussed in Section 2.1, Eq. (39) is written in a coordinate basis aligned along the crystallographic axes. For commonly used (1 0 0) silicon wafers, this amounts to assuming that the waveguide is fabricated along the [0 1 0] or [0 0 1] direction. If that is not the case, the nonlinear response in other Cartesian coordinate systems can be found by a suitable rotation of the basis, resulting in $R'^{(3)}_{ijkl} = R^{(3)}_{qrst} M_{qi} M_{rj} M_{sk} M_{tl}$, where M_{uv} is a rotation matrix. By noting that all terms in Eq. (39) except those involving δ_{ijkl} are rotation invariant, the nonlinear response function in the rotated coordinate system is found to be

$$\begin{aligned} R'^{(3)}_{ijkl}(\tau) = \gamma_e \delta(\tau) \left[\frac{\rho}{3} \left(\delta_{ij}\delta_{kl} + \delta_{ik}\delta_{jl} + \delta_{il}\delta_{jk} \right) + (1-\rho) \sum_s M_{si} M_{sj} M_{sk} M_{sl} \right] \\ + h_R(\tau) \left(\delta_{ik}\delta_{jl} + \delta_{il}\delta_{jk} - 2 \sum_s M_{si} M_{sj} M_{sk} M_{sl} \right). \end{aligned} \tag{42}$$

As an example, consider an SOI waveguide fabricated along the $[0\ \bar{1}\ 1]$ direction because of cleaving convenience. In this case, the new coordinate system is obtained by a 45° rotation

#88416 - $15.00 USD Received 9 Oct 2007; revised 22 Nov 2007; accepted 25 Nov 2007; published 29 Nov 2007

along the x axis, as shown in Fig. 1, and the rotation matrix is given by

$$M = \begin{pmatrix} 1 & 0 & 0 \\ 0 & 1/\sqrt{2} & -1/\sqrt{2} \\ 0 & 1/\sqrt{2} & 1/\sqrt{2} \end{pmatrix}. \tag{43}$$

In this case, it is easy to show that

$$R'^{(3)}_{xxxx}(\tau) = \gamma_e \delta(\tau), \qquad R'^{(3)}_{yyyy}(\tau) = \gamma_e \delta(\tau)(1+\rho)/2 + \gamma_R h_R(\tau), \tag{44}$$

$$R'^{(3)}_{yxxy}(\tau) = R'^{(3)}_{xyyx}(\tau), \qquad R'^{(3)}_{xyyx}(\tau) = \gamma_e \rho\, \delta(\tau)/3 + \gamma_R h_R(\tau). \tag{45}$$

The two components in Eq. (44) represent the nonlinear response of an optical field polarized linearly along the x' and y' axis, respectively, and those in Eq. (45) govern the nonlinear coupling between these two orthogonal polarizations. Two important conclusions can be drawn from Eq. (44) for SOI waveguides fabricated along the $[0\ \bar{1}\ 1]$ direction. First, the Raman contribution is absent for the quasi-TM modes polarized along the x' axis. Second, the electronic contribution is enhanced for the quasi-TE modes by a factor (about 14%) having its origin in the nonlinear anisotropy [87]. Note that Raman scattering can occur for TE modes, but not for TM modes. In contrast, Raman coupling between the pump and signal waves, polarized orthogonally along the TE and TM modes, occurs with the same magnitude, [28, 34, 52] but the Kerr nonlinearity is reduced roughly by one third for such a polarization configuration [80].

In Eq. (37), ξ is related to the frequency dependence of the nonlinear parameter, and is given by

$$\xi \equiv \frac{1}{\omega_0} + \frac{1}{\chi_e(\omega_0)} \left.\frac{d\chi_e}{d\omega}\right|_{\omega_0} - \frac{1}{\bar{a}(\omega_0)} \left.\frac{d\bar{a}}{d\omega}\right|_{\omega_0}, \tag{46}$$

where $\chi_e(\omega_0) \equiv \chi^e_{1111}(-\omega_0; \omega_0, -\omega_0, \omega_0)$. In the 1.55-$\mu$m spectral region, the contribution of the second term in Eq. (46), related to the dispersion of silicon electronic nonlinearity [5, 83, 84], dominates, in contrast with silica fibers for which the first term dominates because of a negligible dispersion of n_2. In practice, the ξ term becomes important only when the spectrum of input pulses broadens by a large factor during their propagation inside a silicon waveguide; for example, in the case of supercontinuum generation [16]. In many cases of practical interest, $\xi \ll 1$, and its contribution can be neglected.

Equation (27) in the frequency domain and Eq. (37) in the time domain provide a general theoretical basis for studying the nonlinear effects in silicon waveguides. We use them in the following sections to discuss a variety of nonlinear phenomena that can be employed for a multitude of practical application of silicon waveguides.

3. SPM effects on short optical pulses

In this section, we apply the general theory to the simplest case in which short optical pulses at a specific carrier wavelength are launched inside a silicon waveguide. The propagation of such pulses is affected considerably by the nonlinear phenomenon of SPM, especially when the dispersive effects cannot be ignored. As Eq. (37) is quite similar to the generalized NLS equation governing the nonlinear effects inside silica fibers [80], we would expect similar phenomena to occur inside a silicon waveguide. In particular, the possibility of soliton formation and supercontinuum generation exists. Of course, the differences unique to silicon waveguides, such as TPA and free-carrier effects, will have a significant impact on these nonlinear phenomena. This section focuses on such differences.

#88416 - $15.00 USD Received 9 Oct 2007; revised 22 Nov 2007; accepted 25 Nov 2007; published 29 Nov 2007

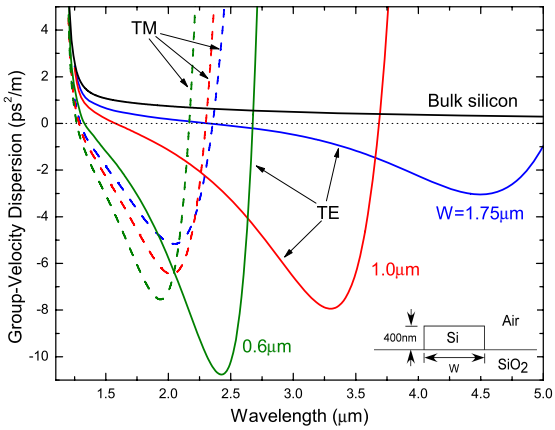

Fig. 2. Wavelength dependence of β_2 for several waveguide widths simulated with the finite-element method (FEMLAB, COMSOL). Solid and dashed curves correspond to the TE and TM modes, respectively. The black curve shows for comparison the case of bulk silicon, and the inset shows the waveguide geometry.

3.1. Dispersion engineering

Before we discuss the SPM effects, we should consider the nature of group-velocity dispersion (GVD) inside SOI waveguides, as it has a profound impact on nonlinear pulse propagation [80]. Fused silica has a zero-dispersion wavelength (ZDWL) around 1.276 μm beyond which GVD becomes anomalous. In contrast, silicon has significant normal dispersion over its transparent spectral region beyond 1.2 μm, as seen in Fig. 2. However, it is well known that mode confinement provided by waveguide geometry introduces significant dispersion, which can be used to compensate for the material dispersion. This feature has been utilized in silica fibers to tailor their dispersion over a broad near-infrared region by either changing the size of the fiber core [147], or by introducing a photonic-crystal cladding [148]. Optical pulses exhibit rich nonlinear dynamics inside such fibers with engineered dispersion [101]. The idea of dispersion engineering can be transferred directly to silicon waveguides. Moreover, as the refractive index of silicon (around 3.48) is much larger than silica glass, mode confinement is naturally stronger in silicon waveguides, particularly those with an air cladding. This feature enables efficient dispersion engineering simply by changing the size and aspect ratio of a rectangular waveguide [13, 149].

In general, the GVD for an optical mode is dominantly set by the boundaries where the electric field is discontinuous. As a result, the quasi-TE modes tend to be more sensitive to the two sidewalls and the waveguide width. In contrast, the quasi-TM modes are more sensitive to the top and bottom interfaces and the waveguide height. This is illustrated clearly in Fig. 2, which shows the wavelength dependence of the GVD parameter β_2, obtained with the finite-element method, for some rectangular-shape waveguides (see the inset). In each case, the height is fixed at 400 nm, but the width W varies from 0.6 to 1.75 μm. As seen there, the waveguide dispersion changes dramatically the magnitude of GVD, and the ZDWL for the fundamental TE mode can be engineered to lie anywhere from 1.2 to beyond 3 μm simply by changing the waveguide width. More specifically, an SOI waveguide with a cross-section of $0.6 \times 0.4\ \mu\mathrm{m}^2$ exhibits its ZDWL near 1328 nm for the fundamental TE mode, resulting in a deeply anomalous GVD in the telecommunication band (about $-1.52\ \mathrm{ps}^2/\mathrm{m}$ at 1550 nm). For the same mode, ZDWL can be tailored to near 1577 nm simply by increasing the waveguide width to 1.0 μm. The ZDWL shifts dramatically to 2322 nm in the mid-infrared region with a further increase

#88416 - $15.00 USD Received 9 Oct 2007; revised 22 Nov 2007; accepted 25 Nov 2007; published 29 Nov 2007

of the width to 1.75 μm, resulting in a normal dispersion of 0.59 ps^2/m at $\lambda = 1550$ nm. In contrast, the GVD curves are similar in shape for the fundamental TM mode (dashed curves) of these three waveguide geometries, because of a fixed waveguide height used. Clearly, the tight mode confinement inside an SOI waveguide provides a significant degree of freedom for engineering GVD.

Further dispersion engineering can be realized by introducing a photonic-crystal cladding, again similar to the case of silica fibers [148]. Such dispersion engineering enables observation of nonlinear phenomena inside a short waveguide at moderate power levels to an extent that is not possible for silica fibers. Moreover, an appropriate design of the waveguide also allows one to obtain nearly identical GVD curves for the two polarizations [68]. The extent of dispersive effects on pulse propagation is characterized by the dispersion length, defined as $L_d = T_0^2/|\beta_2|$ [80], where T_0 is a measure of the width of input pulses. Although the magnitude of GVD can be engineered considerably in SOI waveguides, the dispersion length is still often larger than the waveguide length ($L \sim 1$ cm). For example, for a GVD of $|\beta_2| = 2$ ps^2/m, $L_d = 50$ cm for a pulse with $T_0 = 1$ ps. Therefore, GVD-induced pulse broadening is relatively small until input pulses become shorter than 100 fs.

3.2. Relative magnitudes of the nonlinear and free-carrier effects

As mentioned earlier, the free-carrier effects have a significant impact on pulse propagation. Thus, our first task is to estimate the relative importance of FCA and FCI compared with the nonlinear phenomena of SPM and TPA. The free-carrier effects depend, in general, on the repetition rate of input pulses. In this section, we consider the simplest case and assume that the repetition rate is low enough (<100 MHz) that free carriers produced by one pulse have enough time to recombine before the next pulse arrives. This simplification allows us to focus on a single pulse. Many experiments carried out in the past few years have employed a repetition rate low enough that the single-pulse assumption holds for them [7–12, 14, 15, 17, 23, 25].

The importance of the nonlinear effects is governed by a parameter known as the nonlinear length [80] and defined as $L_N = (\gamma_0 P_0)^{-1}$, where P_0 is the peak power of input pulses. Because of a relatively large value of γ_0 in silicon waveguides, L_N can easily become 1 mm or less at moderate peak power levels. As a result, the SPM-induced spectral broadening is frequently observed in short silicon waveguides [7–12]. Such spectral broadening has already been used to realize useful functions such as optical gating [10], regeneration [19] and multichannel spectral carving [18]. In many cases, a shift of the broadened spectrum toward shorter wavelengths was observed [8–10, 12, 14, 18, 19, 25]. Detailed numerical simulations show that this blue shift is caused by a free-carrier-induced chirp (FCC) that affects pulse dynamics on a different time scale [9, 14, 20–22, 25].

Equation (37) can be used to describe pulse propagation inside SOI waveguides under quite general conditions. For simplifying the following discussion, we do not consider the polarization effects by assuming that the input pulse is polarized along the fundamental TE or TM mode of the waveguide. In this case, the pulse maintains its initial state of polarization, and a scalar approach can be employed in Eq. (37) by dropping the subscript i from A_i. A further simplification occurs if we note that the Raman scattering is not important in this case because of a large Raman shift and a narrowband nature of the Raman-gain spectrum.

Even with these simplifications, the situation is more complicated than that encountered inside silica fibers. Equation (37) shows that both the electronic nonlinearity and free carriers would induce nonlinear phase shifts and extra losses on the pulse. Here we provide a simple analytical approach to estimate their relative magnitudes. Assuming that the dispersion length is so much longer than the waveguide length that dispersive effects are negligible, we neglect

#88416 - $15.00 USD Received 9 Oct 2007; revised 22 Nov 2007; accepted 25 Nov 2007; published 29 Nov 2007

all dispersion terms in Eq. (37) and obtain the simple equation

$$\frac{\partial A}{\partial z} = i\beta^{\mathrm{f}}(\omega_0, \bar{N})A + i\gamma_e|A|^2 A, \tag{47}$$

where we have also neglected linear scattering losses and changed the time reference frame to $\tau = t - \beta_1 z$ so that $\tau = 0$ corresponds to the pulse center.

Consider first the relative importance of the FCA and TPA effects. Noting that the TPA originates from the imaginary part of γ_e in Eq. (40), the power-loss rate introduced by TPA is given by $\partial P/\partial z = -\beta_T |A|^4/\bar{a}$. Accordingly, the carrier generation rate in Eq. (36) becomes

$$\bar{G} = -\frac{1}{2\hbar\omega_0 \bar{a}} \frac{\partial P}{\partial z} = \frac{\beta_T |A|^4}{2\hbar\omega_0 \bar{a}^2}. \tag{48}$$

The use of this expression in Eq. (36) provides a formal solution for the carrier density as

$$\bar{N}(z,\tau) = \frac{\beta_T}{2\hbar\omega_0 \bar{a}^2} \int_{-\infty}^{\tau} e^{-(\tau-\tau')/\tau_0} |A(z,\tau')|^4 d\tau'. \tag{49}$$

Equation (49) shows clearly that carriers accumulate over the pulse duration through TPA, but they also disappear because of recombination. The upper limit of the carrier density is thus the value accumulated over the whole pulse without recombination, and is given by

$$\bar{N}_m = \frac{\beta_T}{2\hbar\omega_0 \bar{a}^2} \int_{-\infty}^{\infty} |A(z,\tau')|^4 d\tau'. \tag{50}$$

To be specific, consider a Gaussian input pulse with the power profile $|A(0,\tau)|^2 = P_0 \exp(-\tau^2/T_0^2)$. In this case, $\bar{N}_m$ becomes

$$\bar{N}_m = \frac{\sqrt{\pi}\beta_T P_0^2 T_0}{2\sqrt{2}\hbar\omega_0 \bar{a}^2}. \tag{51}$$

If we substitute this expression into Eq. (20) and use Eq. (33), we obtain the upper limit α_{fm} of the FCA parameter α_f. As the maximum TPA is governed by $\alpha_{Tm} = \beta_T P_0/\bar{a}$ (at the pulse peak), the ratio of these two provides a criterion for testing the relative magnitudes of FCA and TPA through the dimensionless parameter

$$r_a \equiv \frac{\alpha_{fm}}{\alpha_{Tm}} = \frac{n_0 \sigma_a \mathscr{E}_p}{2\sqrt{2}\hbar\omega_0 n \bar{a}}, \tag{52}$$

where $\mathscr{E}_p = \sqrt{\pi} P_0 T_0$ is the input energy of a Gaussian pulse. Note that n_0 and n are, respectively, the material and modal refractive indices at the carrier frequency ω_0 of the pulse.

It follows from Eq. (52) that the FCA effects are relatively small when $r_a \ll 1$. Using typical parameter values at wavelengths near 1550 nm, Eq. (52) leads to a condition, $\mathscr{E}_p/\bar{a} \ll 25$ mJ/cm^2. For example, pulse energy should satisfy $\mathscr{E}_p \ll 125$ pJ for a waveguide with $\bar{a} = 0.5\ \mu$m^2. This condition is often satisfied in practice for pulses shorter than 0.1 ns. As a result, TPA dominates for ultrashort pulses propagating inside a silicon waveguide. Moreover, α_{fm} is related to r_a as $\alpha_{fm} = r_a \beta_T P_0/\bar{a}$. With $r_a \ll 1$ and $\beta_T \approx 0.5$ cm/GW, $\alpha_{fm} \ll 0.4$ dB/cm at a peak intensity of 0.2 GW/cm^2. Clearly, FCA is negligible for ultrashort pulses of modest energies. However, it can become significant when pulse widths become longer than the carrier lifetime and the peak powers become relatively high. In this case, free carriers created by the leading edge of a pulse would absorb light in the pulse tail. As a result, FCA will dampen the

#88416 - $15.00 USD Received 9 Oct 2007; revised 22 Nov 2007; accepted 25 Nov 2007; published 29 Nov 2007

pulse tail but leave intact the leading part of a pulse. This feature has been recently used to generate short pulses by removing their trailing part through FCA [97].

We next focus on the role played by index changes induced by free carriers (FCI). Both the Kerr nonlinearity and free carriers change the refractive index and impose SPM on the pulse. From Eqs. (20), (33), and (47), these phase changes evolve as

$$\frac{\partial \Phi_K}{\partial z} = \gamma_0 |A|^2, \qquad \frac{\partial \Phi_f}{\partial z} = \frac{n_0 \omega_0 \sigma_n}{cn} \bar{N}, \tag{53}$$

where Φ_K and Φ_f are the phase shifts induced by Kerr nonlinearity and free carriers, respectively. Both of them depend on pulse's temporal profile and thus chirp the pulse. Such frequency chirps are more relevant in practice than the phase shifts themselves since they indicate the extent of spectral broadening [80]. Noting that the frequency shift varies as $\delta\omega = -\partial\Phi/\partial\tau$, the two frequency chirps satisfy

$$\frac{\partial(\delta\omega_K)}{\partial z} = -\gamma_0 \frac{\partial |A|^2}{\partial \tau}, \qquad \frac{\partial(\delta\omega_f)}{\partial z} = -\frac{n_0 \omega_0 \sigma_n}{cn} \frac{\partial \bar{N}}{\partial \tau}. \tag{54}$$

¿From Eqs. (36), (48) and (49), we find that changes in the carrier density evolve as

$$\frac{\partial \bar{N}}{\partial \tau} = \frac{\beta_T}{2\hbar\omega_0 \bar{a}^2} \left[|A|^4 - \frac{1}{\tau_0} \int_{-\infty}^{\tau} e^{-(\tau-\tau')/\tau_0} |A(z,\tau')|^4 d\tau' \right]. \tag{55}$$

Optical pulses used for investigating SPM generally have widths shorter than the carrier lifetime to prevent severe FCA. For such pulses, the second term in Eq. (55) is of the order of T_0/τ_0, and is thus negligible compared with the first term when $T_0 \ll \tau_0$. As a result, the growth rate of FCC from Eq. (54) is approximately given by

$$\frac{\partial(\delta\omega_f)}{\partial z} \approx -\frac{n_0 \sigma_n \beta_T |A|^4}{2cn\hbar\bar{a}^2}. \tag{56}$$

Noting that σ_n is negative [see Eqs. (18) and (20)], it follows that FCC always causes the pulse spectrum to be blue-shifted. The maximum chirp occurs at the pulse center and is given by

$$\frac{\partial(\delta\omega_{fm})}{\partial z} \approx -\frac{n_0 \sigma_n \beta_T P_0^2}{2cn\hbar\bar{a}^2}. \tag{57}$$

On the other hand, the Kerr-induced chirp (KIC) has a maximum growth rate of $|\partial(\delta\omega_{Km})/\partial z| \approx \gamma_0 P_0/T_0$ at two temporal locations around the pulse center [80]. Therefore, the ratio of the FCC and KIC for Gaussian pulses is given by

$$r_c \equiv \frac{|\partial(\delta\omega_{fm})/\partial z|}{|\partial(\delta\omega_{Km})/\partial z|} \approx \frac{n_0 |\sigma_n| \mathscr{E}_p}{4\pi^{3/2} F_n cn\hbar\bar{a}}. \tag{58}$$

Similar to the case of r_a, this ratio depends only on the pulse energy (rather than on pulse width or peak power alone). The FCC and KIC become comparable ($r_c = 1$) for $\mathscr{E}_p/\bar{a} \approx$ 4 mJ/cm^2, or at a pulse energy of $\mathscr{E}_p \approx 20$ pJ for a waveguide with $\bar{a} = 0.5\ \mu$m^2. For pulse energies larger than this value, FCC becomes significant. This condition is easy to meet in practice. For example, the experiments in Refs. [8–10, 12, 14, 18, 19] fall in this regime and result in a blue spectral shift. However, the experiments of Refs. [15, 17] fall outside of this regime and thus do not show such a blue shift. Clearly, compared with FCA, FCC has a more significant effect on pulse propagation, especially when the pulse width is much shorter than the carrier lifetime. Moreover, such FCC can be significantly enhanced inside a high-quality microcavity through cavity resonance, leading to much less requirement of input pulse energy [91, 96].

#88416 - $15.00 USD Received 9 Oct 2007; revised 22 Nov 2007; accepted 25 Nov 2007; published 29 Nov 2007

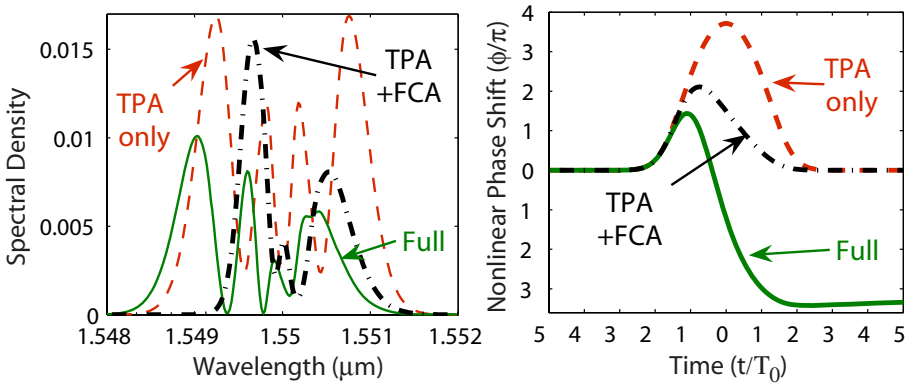

Fig. 3. (a) SPM-broadened spectra and (b) nonlinear phase shifts showing the impact of FCC. Red curves neglect both FCA and FCC, black curves include FCA but neglect FCC, and green curves include both. (After Ref. [21].)

Figure 3 shows numerical examples of SPM-induced spectral broadening and phase shifts for Gaussian pulses with $T_0 = 10$ ps. The device length L and peak power P_0 of pulses are chosen such that $\phi_K = \gamma_0 P_0 L = 15.5\pi$ in the absence of TPA and the resulting free-carrier effects. Red curves neglect both FCA and FCC, assuming negligible density of free carriers. black curves include FCA but neglect FCC, while the green curves include both effects. The blue shift induced by FCC is seen clearly. The free carriers also introduce considerable spectral asymmetry because they are created by the leading edge of the pulse and affect mainly its trailing portion. Notice how the nonlinear phase shift changes from positive to negative values in the tail part of the pulses because of the free-carrier effects.

For relatively low-energy pulses such that $r_c \ll 1$ in Eq. (58), free-carrier effects become negligible. In this case, we can set $\beta^{\rm f} = 0$ in Eq. (47), resulting in

$$\frac{\partial A}{\partial z} = -\frac{\alpha_l}{2}A + i\gamma_e |A|^2 A, \tag{59}$$

where we have added in the term representing linear losses. This equation can be easily solved to obtain the following solution of pulse power:

$$P(z,\tau) = \frac{P(0,\tau)\exp(-\alpha_l z)}{1 + \frac{\beta_T P(0,\tau)}{\alpha_l \bar{a}}\left[1 - \exp(-\alpha_l z)\right]}. \tag{60}$$

Accordingly, the Kerr-induced nonlinear phase shift, $\Phi_K = \gamma_0 \int_0^L P(z,t)\,dz$, is given by [21]

$$\Phi_K(L,\tau) = \frac{\gamma_0 \bar{a}}{\beta_T} \ln\left[1 + \frac{\beta_T P(0,\tau)}{\bar{a}} L_{\rm eff}\right], \tag{61}$$

where $L_{\rm eff} = \left(1 - e^{-\alpha_l L}\right)/\alpha_l$ is the effective length. TPA converts linear dependence of Φ_K on the peak power to a logarithmic one. As a result, it reduces the value of Φ_K by a factor that increases with increasing peak power and sets the fundamental limit on the extent of SPM-induced spectral broadening in silicon waveguides.

3.3. Ultrashort pulse propagation and soliton formation

The preceding analysis neglected the dispersive effects. However, if the dispersion length becomes smaller or comparable to the waveguide length, GVD effects must be considered. If we

#88416 - $15.00 USD Received 9 Oct 2007; revised 22 Nov 2007; accepted 25 Nov 2007; published 29 Nov 2007

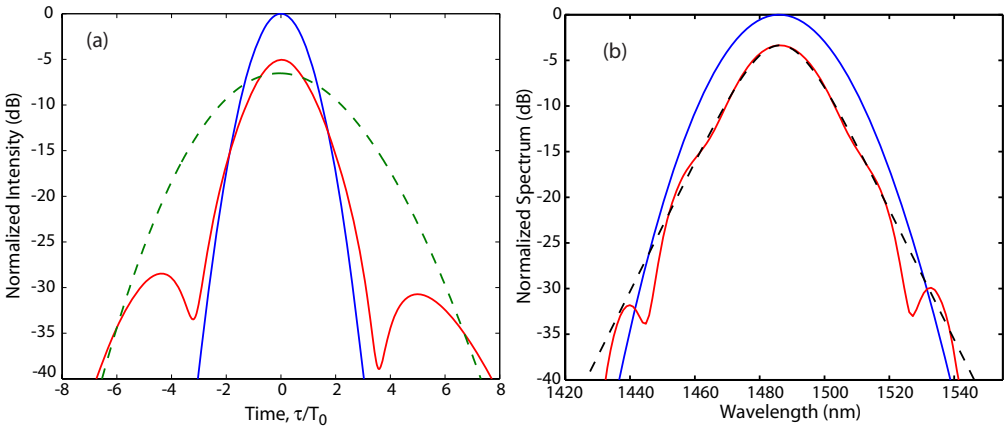

Fig. 4. Simulated shape (a) and spectrum (b) of input (blue curves) and output (red curves) pulses in the soliton regime. The green curve in (a) shows the output pulse in the absence nonlinear effects. The dashed curve in (b) corresponds to a sech pulse. (After Ref. [17].)

keep the GVD term, neglect the high-order dispersive and nonlinear effects, and ignore the impact of free carriers, Eq. (37) reduces to the following simpler NLS equation:

$$\frac{\partial A}{\partial z}+\frac{\alpha_l}{2}A+\frac{i\beta_2}{2}\frac{\partial^2 A}{\partial \tau^2}=i\gamma_e|A|^2A. \tag{62}$$

The main difference compared with optical fibers is that γ_e is a complex parameter in view of the TPA effects that cannot be ignored for silicon waveguides. Since linear losses and TPA reduce the peak power continuously along the waveguide length, an ideal soliton cannot form inside silicon waveguides. However, a soliton-like behavior can still be observed if the SPM effects are made strong enough initially that the dispersion-induced pulse broadening is negligible at the output. Indeed, we have found that if the input pulse is launched with an appropriate peak power, a solitary wave can form with a relatively small pulse broadening [13]. Such a solitary wave corresponds to a path-averaged soliton [80] for which SPM and GVD do not balance each other locally. Rather, they are balanced on average along the whole device length such that $\gamma_0\bar{P}_0L_d=1$, where $\bar{P}_0=L^{-1}\int_0^L P_0(z)dz$ is the average peak power along the waveguide. Under such conditions, an input pulse preserves its temporal and spectral shape reasonably well at the output end [13].

More interestingly, if we launch a Gaussian pulse with an appropriate power in the anomalous GVD regime of an SOI waveguide, the pulse becomes quite resistant to the dispersion-induced broadening [17]. It evolves itself into a sech-like shape, as shown clearly in the numerical example of Fig. 4. In this case, the pulse spectrum narrows down since the Gaussian-shape input spectrum is too broad to hold a solitary wave. This feature is in strong contrast to the case of nondispersive SPM (discussed earlier) that resulted in spectral broadening.

Spectral narrowing suggesting the formation of a path-averaged soliton was observed in a recent experiment in which 120-fs Gaussian pulses were launched in the anomalous-GVD regime of an SOI waveguide [17]. As shown in Fig. 5, the 27.8-nm-wide (FWHM) spectrum of input pulses is narrowed by about 33% at the output end. The shape of the output spectrum is best described by a sech shape, rather than a Gaussian. Numerically simulations performed with the experimental parameters fit the experimental spectrum reasonably well, as seen in Fig. 5(b).

#88416 - $15.00 USD Received 9 Oct 2007; revised 22 Nov 2007; accepted 25 Nov 2007; published 29 Nov 2007

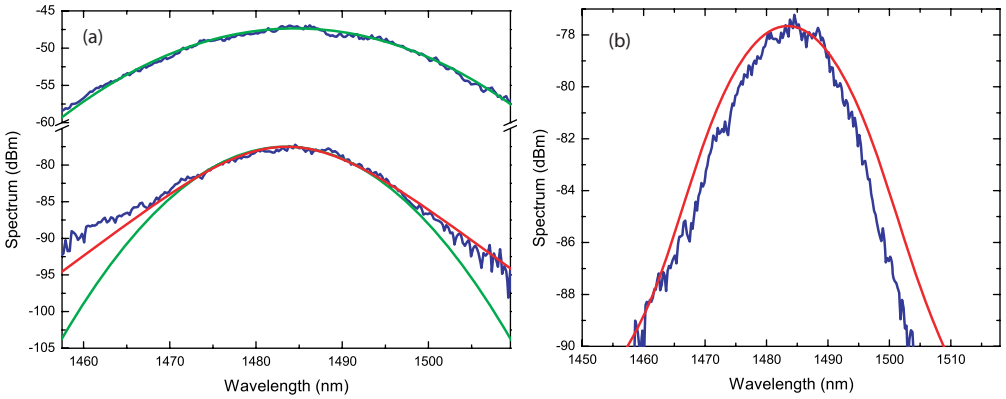

Fig. 5. (a) Measured spectra (blue curves) at the input and output ends for Gaussian pulses. The green and red curves show the Gaussian and 'sech' fits to the data. Part (b) shows a numerical fit to the output spectrum. (After Ref. [17].)

3.4. Soliton fission and supercontinuum generation

Spectral broadening introduced by SPM can be used for applications such as multichannel spectral carving [18]. This technique may find applications in the context of optical interconnects based on the scheme of wavelength-division multiplexing. However, as discussed above, spectral broadening introduced by the sole effect of SPM is quite limited because TPA imposes a fundamental limit on the extent of such broadening. Current experiments only show spectral broadening of tens of nanometers [7–10, 12, 14, 25].

To overcome the barrier set by TPA, an optical pulse needs to broaden its spectrum by a large factor before TPA reduces its peak power. This can be done by employing the concept of soliton fission and supercontinuum generation, two processes that have been extensively studied for silica fibers in the past few years [101]. Spectral broadening is enhanced dramatically by forming a higher-order soliton at the input end of the waveguide that splits into multiple fundamental solitons through a fission process. In general, Eq. (27), which includes all possible linear and nonlinear effects and wave-mixing processes, should be used to simulate the dramatic spectral broadening during supercontinuum generation. In particular, the spectral dependence of the propagation constant $\beta_i(\omega)$ should be accurately accounted for across the entire broadened spectral region because the soliton fission process is very sensitive to high-order dispersion [101]. In practice, the generalized time-domain NLS equation (37) provides a fairly accurate description of such spectral broadening if correctly including in higher-order linear dispersion terms together with the nonlinear dispersion of Eq. (46).

Numerical simulations typically make use of the split-step Fourier method [80] that deals with dispersion in the frequency domain and treats SPM in the time domain. It is thus relatively easy to include higher-order dispersive effects. The results show that the soliton fission process can generate a supercontinuum that extends over 400 nm even for a 3-mm-long SOI waveguide [16]. Figure 6 shows the supercontinuum created when a 50-fs pulse is launched to excite a third-order soliton inside the waveguide. Although TPA and free carriers reduce the total bandwidth, a 400-nm-wide spectrum could be generated in spite of them. Such wide spectra have not yet been observed experimentally, but recent experiments have shown evidence of the emission of dispersive waves from an optical pulse under the impact of third-order dispersion [15, 23]. This process enhances spectral broadening, and it also provides a simple way to characterize the third-order dispersion.

#88416 - $15.00 USD Received 9 Oct 2007; revised 22 Nov 2007; accepted 25 Nov 2007; published 29 Nov 2007

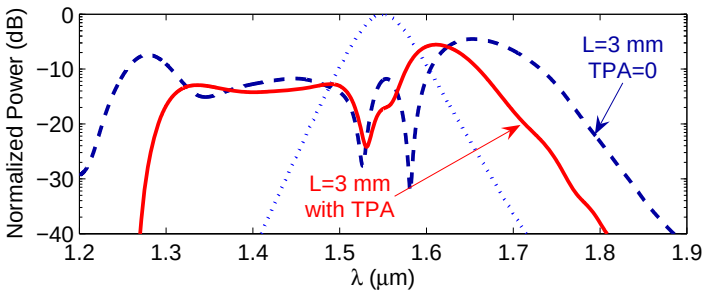

Fig. 6. Supercontinuum created inside a 3-mm-long SOI waveguide when a 50-fs pulse excites the third-order soliton (red curve). The blue curve ignores the effects of TPA and FCA are ignored. The dotted curve shows the input pulse spectrum. (After Ref. [16].)

4. XPM and Raman interactions involving two waves

The situation becomes considerably more complicated when two optical waves with different wavelengths, and possibly different states of polarization, copropagate inside a silicon waveguide. For example, SRS may occur if the wavelength difference matches the Raman shift. Even when the Raman effects are not important, XPM couples the two waves and results in a variety of new effects [80]. To include the possibility of Raman scattering, we consider two waves copolarized along the TE mode of a waveguide, fabricated along the $[0\ \bar{1}\ 1]$ direction.

The starting point in this case is the frequency-domain NLS equation (27). By writing the total field in the form $\widetilde{A}_i(z,\omega) = \widetilde{A}_p(\omega-\omega_p) + \widetilde{A}_s(\omega-\omega_s)$, where the subscripts p and s denote the pump and signal waves, respectively, decomposing the equation into equations for individual waves, and converting the resulting equations to time domain, we obtain the following two coupled NLS equations:

$$\frac{\partial A_p}{\partial z} - i\sum_{m=0}^{\infty}\frac{i^m\beta_{mp}}{m!}\frac{\partial^m A_p}{\partial t^m} = -\frac{\alpha_{lp}}{2}A_p + i\beta_p^f A_p + i\left\{\gamma_{pp}(0)|A_p|^2 + \left[\gamma_{ps}^e + \gamma_{ps}(0)\right]|A_s|^2\right\}A_p + i\gamma_{ps}^R A_s\int_{-\infty}^{t} h_R(t-t')e^{i\Omega_{ps}(t-t')}A_s^*(z,t')A_p(z,t')dt', \tag{63}$$

$$\frac{\partial A_s}{\partial z} - i\sum_{m=0}^{\infty}\frac{i^m\beta_{ms}}{m!}\frac{\partial^m A_s}{\partial t^m} = -\frac{\alpha_{ls}}{2}A_s + i\beta_s^f A_s + i\left\{\gamma_{ss}(0)|A_s|^2 + \left[\gamma_{sp}^e + \gamma_{sp}(0)\right]|A_p|^2\right\}A_s + i\gamma_{sp}^R A_p\int_{-\infty}^{t} h_R(t-t')e^{i\Omega_{sp}(t-t')}A_p^*(z,t')A_s(z,t')dt', \tag{64}$$

where α_{lv} ($v = p,s$) is linear loss at the carrier frequency ω_v, $\beta_{mv} = \beta_m(\omega_v)$ accounts for various orders of dispersion, $\beta_v^f \equiv \beta^f(\omega_v,\bar{N})$ governs the free-carrier effects, and $\Omega_{uv} \equiv \omega_u - \omega_v$ represents the frequency detuning. We have assumed that the pulses are long enough that the higher-order nonlinear terms can be neglected. In Eqs. (63) and (64), the nonlinear parameter γ_{uv} includes both electronic and Raman contributions as $\gamma_{uv}(\Omega) \equiv \gamma_{uv}^e + \gamma_{uv}^R\widetilde{H}_R(\Omega)$. Similar to the case of single-pulse propagation, the Raman nonlinear parameter is related to the Raman gain coefficient as $\gamma_{uv}^R = g_R(\omega_u)\Gamma_R/(\bar{a}_{uv}\Omega_R)$, where the effective mode area $\bar{a}_{uv} = \sqrt{a_u a_v}$ is obtained from Eq. (29). The Raman gain coefficient is obtained from Eqs. (2) and (28) and is given by

$$g_R(\omega_u) = \frac{3\omega_u g'\Omega_R\eta_{uv}}{2\varepsilon_0 c^2 n_u n_v \Gamma_R}, \tag{65}$$

where the mode overlap factor $\eta_{uv} \equiv \eta_{uvvu}$ is given by Eq. (30). Note that g_R scales linearly with optical frequency. When $\omega_u = \omega_v$, γ_{uv}^R and $g_R(\omega_u)$ reduce to the single-wave case discussed

#88416 - $15.00 USD Received 9 Oct 2007; revised 22 Nov 2007; accepted 25 Nov 2007; published 29 Nov 2007

in Section 3. For the TE mode polarized along the $[0\ \bar{1}\ 1]$ direction, the electronic nonlinear parameter is given by

$$\gamma^e_{\rm uv} = \gamma^e_{1111}(-\omega_u;\omega_v,-\omega_v,\omega_u)(1+\rho)/2. \tag{66}$$

As discussed previously, since $\gamma^R_{\rm uv}$ scales with Γ_R/Ω_R, its value is only a few percent of the electronic part $\gamma^e_{\rm uv}$. As a result, $\gamma_{\rm uv}(0) \approx \gamma^e_{uv}$.

4.1. XPM and cross two-photon absorption

If the frequency detuning between the two waves is far from the Raman frequency shift, the terms involving the Raman response function $h_R(t)$ in Eqs. (63) and (64) are irrelevant. For picosecond optical pulses, dispersion length is typically much longer than the waveguide length, and the dispersion terms ($m > 1$) are also negligible in these equations, resulting in

$$\frac{\partial A_p}{\partial z} + \beta_{1p}\frac{\partial A_p}{\partial t} = i\beta^{\rm f}_p A_p + i\left(\gamma^e_{\rm pp}|A_p|^2 + 2\gamma^e_{\rm ps}|A_s|^2\right)A_p, \tag{67}$$

$$\frac{\partial A_s}{\partial z} + \beta_{1s}\frac{\partial A_s}{\partial t} = i\beta^{\rm f}_s A_s + i\left(\gamma^e_{\rm ss}|A_s|^2 + 2\gamma^e_{\rm sp}|A_p|^2\right)A_s, \tag{68}$$

where we neglected the terms associated with $\gamma^R_{\rm uv}$ because of its small magnitude and used $\gamma_{\rm uv}(0) \approx \gamma^e_{\rm uv}$. We also neglected linear losses and removed the trivial constant phase factor $e^{i\beta_{0v}z}$ ($v = p,s$). These two equations are similar to those describing the XPM effects in silica fibers, except for the TPA and free-carrier terms [80]. As a result, we may expect that XPM inside a silicon waveguide should exhibit similar spectral characteristics. This indeed was observed recently by using femtosecond pulses [14, 26]. In particular, the XPM-induced spectral asymmetry because of a pump-probe delay was seen clearly, and its features agreed with theory. Similar to the case of silica fibers [116], the XPM-induced phase shift and its associated chirp can be used for optical switching and wavelength conversion [14, 25].

The TPA effects can be deduced from Eqs. (67) and (68) by studying how the powers, $P_p = |A_p|^2$ and $P_s = |A_s|^2$, change along the waveguide length. These powers satisfy the following set of two coupled equations:

$$\frac{\partial P_p}{\partial z} + \beta_{1p}\frac{\partial P_p}{\partial t} = -\beta'_{\rm Tpp}P_p^2 - 2\beta'_{\rm Tps}P_sP_p, \tag{69}$$

$$\frac{\partial P_s}{\partial z} + \beta_{1s}\frac{\partial P_s}{\partial t} = -\beta'_{\rm Tss}P_s^2 - 2\beta'_{\rm Tsp}P_sP_p, \tag{70}$$

where the TPA coefficient is defined as $\beta'_{\rm Tuv} \equiv 2{\rm Im}(\gamma^e_{\rm uv}) \equiv \beta_{\rm Tuv}/\bar{a}_{\rm uv}$. These equations show that TPA can occur in three ways: by absorbing two pump photons, two signal photons, or one pump and one signal photon (cross-TPA). The factor of 2 for the last process arises from the interference effects and the instantaneous nature of the TPA process [150]. Noting that $\chi^e_{1111}(-\omega_p;\omega_s,-\omega_s,\omega_p) = \chi^e_{1111}(-\omega_s;\omega_p,-\omega_p,\omega_s)$, from Eqs. (28) and (66), we find that

$$\frac{\beta'_{\rm Tps}}{\omega_p} = \frac{\beta'_{\rm Tsp}}{\omega_s}, \tag{71}$$

irrespective of the pump and signal frequencies. Physically, this equality indicates that cross-TPA annihilates one pump and one signal photon simultaneously. Taking into account the three TPA processes, the free-carrier generation rate in Eq. (36) is given by

$$\bar{G} = \frac{\beta_{\rm Tpp}|A_p|^4}{2\hbar\omega_p\bar{a}^2_{\rm pp}} + \frac{\beta_{\rm Tss}|A_s|^4}{2\hbar\omega_s\bar{a}^2_{\rm ss}} + \frac{2\beta_{\rm Tps}|A_p|^2|A_s|^2}{\hbar\omega_p\bar{a}^2_{\rm ps}}, \tag{72}$$

#88416 - $15.00 USD Received 9 Oct 2007; revised 22 Nov 2007; accepted 25 Nov 2007; published 29 Nov 2007

where the self-TPA coefficient β_{Tpp} and β_{Tss} are given in Eq. (8) for degenerate frequency ω_p and ω_s, respectively. The cross-TPA coefficient β_{Tps} is measurable in principle but it has not yet been measured for silicon. A good approximation is to estimate it at the mean frequency $\bar{\omega} = (\omega_p + \omega_s)/2$ as $\beta_{\mathrm{Tps}} \approx \beta_{\mathrm{T}}(\bar{\omega})$, because the TPA process is most sensitive to the total energy of the two absorbed photons [128]. As self-TPA coefficient does not show sharp dependence on photon energy below E_g [83, 84], $\beta_{\mathrm{Tpp}} \approx \beta_{\mathrm{Tss}} \approx \beta_{\mathrm{Tps}}$ when frequencies ω_p and ω_s are close to each other.

Equation (72) shows that cross-TPA-induced carriers and the associated photocurrent are generated only when both pulses are present simultaneously. This feature enables the use of cross-TPA for measuring the temporal characteristics of ultrashort optical pulses [151–156] and employing it for ultrafast optical switching [98–100]. However, as the cross-TPA generation rate is only four times larger than that of self-TPA, each pulse by itself also generates a considerable number of carriers [the first two terms in Eq. (72)]. As a result, the autocorrelation based on cross-TPA is generally not background free, unless a specific technique is used to remove the background [157].

Apart from the XPM induced by the Kerr nonlinearity, TPA-generated free carriers induce additional phase modulation through index changes produced by free carriers. From Eqs. (20), (33), and (68), these phase shifts for a pump-probe configuration ($P_s \ll P_p$) satisfy

$$\frac{\partial \Phi_K}{\partial z} = 2\mathrm{Re}(\gamma_{\mathrm{sp}}^e)|A_p|^2, \qquad \frac{\partial \Phi_f}{\partial z} = \frac{n_{0s}\omega_s}{cn_s}\sigma_{ns}\bar{N}. \tag{73}$$

The Kerr-induced XPM has a maximum growth rate of $\partial\Phi_{Km}/\partial z = 2\mathrm{Re}(\gamma_{\mathrm{sp}}^e)P_0$ at the pulse center. For a Gaussian pump pulse much shorter than the carrier lifetime, the maximum rate of carrier-induced XPM can be estimated by using Eq. (51) in Eq. (73) and is given by

$$\frac{\partial \Phi_{fm}}{\partial z} = \frac{\sqrt{\pi} n_{0s}\omega_s\sigma_{ns}\beta_{\mathrm{Tpp}}P_0^2 T_0}{2\sqrt{2}cn_s\hbar\omega_p\bar{a}_{\mathrm{pp}}^2}. \tag{74}$$

The relative ratio of the growth rates of these two phase modulations is given by

$$r_x \equiv \frac{|\partial\Phi_{fm}/\partial z|}{|\partial\Phi_{Km}/\partial z|} = \frac{n_{0s}\omega_s|\sigma_{ns}|\beta_{\mathrm{Tpp}}\mathscr{E}_p}{4\sqrt{2}cn_s\mathrm{Re}(\gamma_{\mathrm{sp}}^e)\hbar\omega_p\bar{a}_{\mathrm{pp}}^2} \approx \frac{\sqrt{\pi}r_c}{2\sqrt{2}}, \tag{75}$$

where r_c is given in Eq. (58) and the last approximation is valid when the pump and signal frequencies are not too far from each other. Clearly, the discussion about r_c in the preceding section applies to r_x as well. As this ratio is typically much larger than 1 for moderate pump-pulse energies, free-carrier-induced XPM provides a more efficient way for optical switching, particularly when an interferometric resonance inside a micro-resonator is used to enhance such effects [90, 92]. However, this carrier-injection scheme has a speed limited by the carrier lifetime (typically ~1 ns) [94], and it responds much slower compared with a scheme based on Kerr-induced XPM or TPA. The modulation speed can be increased considerably by reducing the effective carrier lifetime. This is often realized by applying an external field to swipe away the free carriers [92].

4.2. Raman amplification and lasing

When the frequency detuning between the pump and signal becomes close to the Raman shift, SRS begins to affect the pulse propagation. As the Raman response time is about 3 ps, SRS is only effective for pulses longer than this. Through a pump-probe scheme, 6-dB and 6.8-dB gains were observed in experiments employing 3.5-ps and 6.6-ps-wide pump pulses, respectively [31, 34]. Numerical simulations show that a signal pulse can grow even from noise [47].

#88416 - $15.00 USD Received 9 Oct 2007; revised 22 Nov 2007; accepted 25 Nov 2007; published 29 Nov 2007

However, for such short pump pulses, SRS process is affected by the walk-off between the pump and signal pulses [47, 48] because the group-velocity mismatch is not negligible for a Raman shift of 15.6 THz. This walk-off problem can be solved by launching a CW signal [32, 40, 44]. Indeed, a net Raman gain of 2 [32], 3.1 [40] and 13 dB [44] was observed in three such experiments. Raman lasing has also been realized through pulsed pumping [38, 43].

However, practical applications generally require CW pumping. In this case, both the TPA and FCA affect the SRS process considerably. To study their impact, we employ Eqs. (63) and (64). The time integral in these equations is readily performed for CW fields, resulting in

$$\frac{\partial A_p}{\partial z} = i\beta_p A_p - \frac{\alpha_{\rm lp}}{2}A_p + i\beta_p^{\rm f}A_p + i\left\{\gamma_{\rm pp}(0)|A_p|^2 + [\gamma_{\rm ps}(0)+\gamma_{\rm ps}(\Omega_{\rm ps})]|A_s|^2\right\}A_p, \quad (76)$$

$$\frac{\partial A_s}{\partial z} = i\beta_s A_s - \frac{\alpha_{\rm ls}}{2}A_s + i\beta_s^{\rm f}A_s + i\left\{\gamma_{\rm ss}(0)|A_s|^2 + [\gamma_{\rm sp}(0)+\gamma_{\rm sp}(\Omega_{\rm sp})]|A_p|^2\right\}A_s. \quad (77)$$

We are mainly interested in studying how the pump and signal powers, P_p and P_s, evolve along the waveguide length. These powers satisfy the following coupled equations:

$$\frac{\partial P_p}{\partial z} = -(\alpha_{\rm lp}+\alpha_{\rm fp})P_p - \beta'_{\rm Tpp}P_p^2 - 2\beta'_{\rm Tps}P_sP_p - 2\gamma^R_{\rm ps}{\rm Im}[\widetilde{H}_R(\Omega_{\rm ps})]P_sP_p, \quad (78)$$

$$\frac{\partial P_s}{\partial z} = -(\alpha_{\rm ls}+\alpha_{\rm fs})P_s - \beta'_{\rm Tss}P_s^2 - 2\beta'_{\rm Tsp}P_pP_s - 2\gamma^R_{\rm sp}{\rm Im}[\widetilde{H}_R(\Omega_{\rm sp})]P_pP_s, \quad (79)$$

where $\widetilde{H}_R(\Omega)$ is given in Eq. (3). When the signal is located at the Stokes side of the pump with a frequency detuning of the Raman shift, $\Omega_{\rm sp} = -\Omega_R$, Eq. (3) and Eq. (79) result in a peak Raman gain of $g_R(\omega_s)/\bar{a}_{\rm sp}$ where $g_R(\omega_s)$ is given in Eq. (65).

As expected, apart from the gain or loss provided by the SRS process, the two waves suffer losses from the TPA and FCA processes. In the following analysis, we assume that the pump is much more intense than the signal so that free carriers are dominantly generated from the pump-induced TPA. In this case, Eqs. (20), (33), and (49) show that FCA coefficient is given by

$$\alpha_{\rm fs} = \frac{n_{0s}\sigma_{as}\beta_{\rm Tpp}\tau_0 P_p^2}{2\hbar\omega_p n_s \bar{a}_{\rm pp}^2}. \quad (80)$$

In the CW pumping case, it turns out that FCA is the dominant loss mechanism rather than TPA [32–36]. This can be seen from the loss ratio defined in Eq. (52). In the steady state with CW pumping, Eq. (52) becomes

$$r_a = \frac{n_{0s}\sigma_{as}\beta_{\rm Tpp}P_p\tau_0\bar{a}_{\rm sp}}{4\hbar\omega_0 n_s\beta_{\rm Tsp}\bar{a}_{\rm pp}^2}. \quad (81)$$

Using $\beta_{\rm Tsp}\approx\beta_{\rm Tpp}$ and $\bar{a}_{\rm sp}\approx\bar{a}_{\rm pp}$, we find from Eq. (81) that $r_a > 1$ at a moderate power level of $P_p/\bar{a}_{\rm sp} > 35$ MW/cm^2 for an SOI waveguide with $\tau_0 = 1$ ns. To realize a Raman amplification, we need $g_R P_p L/\bar{a}_{\rm sp} > 1$, which leads to the requirement $P_p/\bar{a}_{\rm sp} > 50$ MW/cm^2. Clearly, FCA is the major obstacle for Raman amplification.

As a rough estimate of the combined effects of SRS, FCA, and TPA, assume that the signal is located at Raman gain peak, Eq. (79) together with Eq. (80) shows that net amplification of the signal through SRS is possible only when

$$(g_R - 2\beta_{\rm Tsp})\frac{P_p}{\bar{a}_{\rm sp}} - \frac{n_{0s}\sigma_{as}\beta_{\rm Tpp}\tau_0 P_p^2}{2\hbar\omega_p n_s\bar{a}_{\rm pp}^2} - \alpha_{\rm ls} > 0. \quad (82)$$

#88416 - $15.00 USD Received 9 Oct 2007; revised 22 Nov 2007; accepted 25 Nov 2007; published 29 Nov 2007

This quadratic relation and the requirement that P_p is a real positive quantity lead to the following condition on the carrier lifetime:

$$\tau_0 < \tau_{\rm th} \equiv \frac{\hbar\omega_p n_s \bar{a}_{\rm pp}^2 (g_R - 2\beta_{\rm Tsp})^2}{2\alpha_{\rm ls}\sigma_{as} n_{0s}\beta_{\rm Tpp}\bar{a}_{\rm sp}^2}. \tag{83}$$

This condition imposes a stringent limitation on the carrier lifetime for net Raman amplification. For example, using typical parameter values with $\beta_{\rm Tsp} \approx \beta_{\rm Tpp}$, the carrier lifetime should be <60 ns for a waveguide with a low linear loss of 0.2 dB/cm. Indeed, positive Raman amplification with CW pumping was observed inside a waveguide with a linear loss of 0.22 dB/cm and a carrier lifetime of 25 ns [33]. However, as smaller values of τ_0 are required with increasing linear losses, Eq. (83) is hard to satisfy for practical silicon waveguides because a low loss available for large waveguides also leads to longer carrier lifetimes. Decreasing the waveguide cross section helps reduce the carrier lifetime [139], but it also increases scattering losses. The real situation is worse than the rough estimate in Eq. (83) because FCA and TPA also reduce the pump power along the waveguide that was assumed to remain constant. In this case, Eq. (82) should be replaced with

$$\frac{(g_R - 2\beta_{\rm Tsp})}{\bar{a}_{\rm sp}} \int_0^L P_p dz - \frac{n_{0s}\sigma_{as}\beta_{\rm Tpp}\tau_0}{2\hbar\omega_p n_s \bar{a}_{\rm pp}^2} \int_0^L P_p^2 dz - \alpha_{\rm ls} L > 0. \tag{84}$$

As a relatively low effective lifetime of free carriers in SOI waveguides is critical for practical application of Raman amplification, significant efforts have bee made to reduce its magnitude. For example, the effective lifetime could be reduced in one experiment from 100 ns to 1.9 ns through helium-ion implantation, thereby enabling positive Raman amplification [140]. In another approach, free carriers are quickly swept away from the core area by applying an external dc field [41, 42, 45, 54, 56]. Indeed, efficient Raman amplification realized with this approach has been used to make CW silicon Raman lasers with a threshold as low as 20 mW [41, 42, 54].

The lasing threshold can be estimated from Eq. (84) by setting its left side equal to zero. In this case, the linear loss factor $\alpha_{\rm ls}$ should be replaced by total distributed cavity losses $\alpha_{\rm ts}$ that include coupling losses and reflection from cavity mirrors. It turns out that there is an upper limit on the carrier lifetime above which the Raman laser would not be able to operate, no matter how large the pump power is [39]. This can be seen clearly from Eqs. (82) and (83) after replacing $\alpha_{\rm ls}$ with $\alpha_{\rm ts}$. Equation (82) cannot be satisfied for any pump power, if τ_0 is larger than $\tau_{\rm th}$ given in Eq. (83). If cavity losses are small (*e.g.*, in the case of a microcavity), the lasing threshold is found from Eq. (82) to be

$$P_{\rm th} = \frac{\omega_p \omega_s n_{\rm gp} n_{\rm gs} V_m}{2c^2(g_R - 2\beta_{\rm Tsp})} \frac{Q_{\rm ep}}{Q_{\rm ts} Q_{\rm tp}^2} \frac{\tau_{\rm th}}{\tau_0} \left[1 - \left(1 - \frac{\tau_0}{\tau_{\rm th}}\right)^{1/2}\right], \tag{85}$$

where $V_m = \bar{a}_{\rm sp} L$ is the effective mode volume, $n_{\rm gv}$ is the group index at ω_v ($v = p, s$), and $Q_{\rm ev}$ and $Q_{\rm tv}$ are the external and loaded quality factors for the cavity, respectively. They are related to linear loss as $Q_{\rm uv} = n_{\rm gv}\omega_v/(c\alpha_{\rm uv})$ ($u = e, t$), where $\alpha_{\rm ev}$ is linear coupling loss at ω_v.

Equation (85) shows clearly that lasing is possible only when $\tau_0 < \tau_{\rm th}$. If the carrier lifetime is small enough that $\tau_0 \ll \tau_{\rm th}$, Eq. (85) leads to

$$P_{\rm th} = \frac{\omega_p \omega_s n_{\rm gp} n_{\rm gs} V_m}{4c^2(g_R - 2\beta_{\rm Tsp})} \frac{Q_{\rm ep}}{Q_{\rm ts} Q_{\rm tp}^2}, \tag{86}$$

This expression reduces to the case of microcavities when TPA is negligible [158]. However, if the carrier lifetime approaches $\tau_{\rm th}$, Eq. (85) shows that the lasing threshold becomes twice

#88416 - $15.00 USD Received 9 Oct 2007; revised 22 Nov 2007; accepted 25 Nov 2007; published 29 Nov 2007

of that given in Eq. (86). Of course, as the pump itself starts to experience significant losses, the real threshold would more than double in practice [39]. Similar to the case of Raman lasing in microcavities [158], Eq. (85) shows that the lasing threshold is linearly proportional to effective mode volume and inversely proportional to the square of the cavity Q factor. As a result, increasing the Q factor or reducing the mode volume would significantly lower the lasing threshold in Raman lasers built using SOI waveguides.

It is important to note that the inequalities in Eqs. (82) and (84) can only be satisfied for a certain range of pump powers. In practical terms, FCA would always cause the Raman amplification/lasing to saturate and thus limit the maximum available output power. The upper limit of pump power for Raman lasers can be estimated from Eq. (82) and is given by:

$$P_{\mathrm{m}} = \frac{\omega_p \omega_s n_{\mathrm{gp}} n_{\mathrm{gs}} V_m}{2c^2 (g_R - 2\beta_{\mathrm{Tsp}})} \frac{Q_{\mathrm{ep}}}{Q_{\mathrm{ts}} Q_{\mathrm{tp}}^2} \frac{\tau_{\mathrm{th}}}{\tau_0} \left[1 + \left(1 - \frac{\tau_0}{\tau_{\mathrm{th}}} \right)^{1/2} \right]. \tag{87}$$

This equation shows clearly that $P_{\mathrm{m}} \to \infty$ when $\tau_0 \ll \tau_{\mathrm{th}}$, and the lasing saturation is negligible. However, as τ_0 becomes close to τ_{th}, the maximum allowed pump power P_{m} approaches P_{th}. Eventually, the power range to obtain positive intracavity gain becomes so small that Raman lasing is quenched.

The preceding simple analytical theory explains qualitatively the observed features of Raman silicon lasers [39, 41, 42, 54]. A similar discussion can be found in [58]. A quantitative description of such lasers requires numerical simulations based on Eqs. (78) and (79). Note that the lasing in general can occur in both the forward and backward directions. Thus, an accurate quantitative description of silicon Raman lasers requires numerical simulations of three equations [39], or even four equations if the pump wave also propagates along both directions [59]. More technical details about Raman lasers can be found in two recent reviews [52, 53].

Apart from the power amplification, SRS is a resonant process that also changes the refractive index of silicon itself. From Eqs. (3), (76) and (77), the Raman-induced perturbation to the propagation constant is given by

$$\beta_R = \frac{g_R P_p \Gamma_R \Omega_R}{\bar{a}_{\mathrm{sp}}} \frac{\Omega_R^2 - \Omega^2}{(\Omega_R^2 - \Omega^2)^2 + 4\Gamma_R^2 \Omega^2}. \tag{88}$$

This quantity is positive (negative) when the pump-signal detuning is smaller (larger) than the Raman frequency shift. Physically, this stems from the fact of a standard resonant system that stimulated lattice vibrations follow the pump-signal beating in phase (out of phase) when the beating frequency is smaller (larger) than the resonant frequency. As the Raman gain spectrum is relatively narrow, such changes of propagation constant within the Raman gain spectrum lead to dramatic changes in the group velocity. In particular, the group delay at the center of the Raman gain spectrum is given by

$$\tau_g = \frac{g_R}{2\Gamma_R \bar{a}_{\mathrm{sp}}} \int_0^L P_p(z) dz. \tag{89}$$

The magnitude of Raman-induced group delay is directly proportional to the pump power. This feature provides tunable delays simply by changing the pump power [50,51]. Interestingly, such Raman-induced group delays exist even when no net Raman amplification occurs (TPA and FCA depend on frequency only weakly and introduce a negligible change in group velocity). This scheme was recently used to demonstrate a tunable group delay of up to 4 ps [51].

5. FWM and its applications

The situation becomes more complicated in the case of FWM because three or four waves co-propagate inside an SOI waveguide simultaneously. Only three waves are involved in the case of

#88416 - $15.00 USD Received 9 Oct 2007; revised 22 Nov 2007; accepted 25 Nov 2007; published 29 Nov 2007

degenerate FWM. These are called the pump, signal, and idler waves, and their photon energies satisfy the energy-conservation relation $2\hbar\omega_p = \hbar\omega_s + \hbar\omega_i$. As this process is a four-photon, elastic scattering process originating from the Kerr nonlinearity, its instantaneous nature makes it useful for a variety of applications related to ultrafast optical signal processing using silica fibers [159]. The possibility of using FWM in silicon waveguides for similar applications has excited considerable interest recently [61–75, 77–79, 137].

5.1. Free-carrier effects on FWM

As seen in preceding sections, free carriers introduce considerable loss and phase modulation, and thus impact any nonlinear interaction inside a silicon waveguide. Indeed, the density of TPA-created free carriers becomes large enough in some cases that the reuse of their energy was proposed recently [160, 161]. Clearly, free carriers would affect the FWM process as well. Before discussing the details of FWM, we first look into the impact of free carriers.

It turns out that most free-carrier effects on FWM can be deduced from Eq. (37). For simplicity, we first assume that all optical waves are polarized along the TM mode so that Raman scattering is absent. By using Eqs. (20), (33) and (49) in Eq. (37), we obtain

$$\frac{\partial A}{\partial z} = \sum_{m=0}^{\infty} \frac{i^{m+1}\beta_m}{m!}\frac{\partial^m A}{\partial t^m} + i\gamma_e|A|^2A + i\gamma_f A\int_{-\infty}^{t} e^{-(t-t')/\tau_0}|A(z,t')|^4dt', \tag{90}$$

where the parameter γ_f is defined as

$$\gamma_f = \frac{\beta_T}{2\hbar\omega_0\vec{a}^2}\frac{n_0(\omega_0)}{n(\omega_0)}\left[\frac{\omega_0}{c}\sigma_n(\omega_0) + \frac{i}{2}\sigma_a(\omega_0)\right]. \tag{91}$$

Equation (90) shows clearly that TPA-induced free carriers produce a fifth-order nonlinear effect that is accumulative in nature [115].

To describe the FWM process, we assume that $A(z,t)$ is composed of three waves such that $A(z,t) = A_p(z,t)e^{-i\omega_p t} + A_s(z,t)e^{-i\omega_s t} + A_i(z,t)e^{-i\omega_i t}$, among which the pump field A_p is much more intense than the signal A_s and idler A_i. We substitute this expression into Eq. (90) and obtain the following three equations at individual frequencies:

$$\frac{\partial A_p}{\partial z} - i\sum_{m=0}^{\infty}\frac{i^m\beta_{mp}}{m!}\frac{\partial^m A_p}{\partial t^m} = i\gamma_e|A_p|^2A_p + i\gamma_f A_p\int_{-\infty}^{t} e^{-(t-t')/\tau_0}|A_p(z,t')|^4dt', \tag{92}$$

$$\begin{aligned}\frac{\partial A_s}{\partial z} - i\sum_{m=0}^{\infty}\frac{i^m\beta_{ms}}{m!}\frac{\partial^m A_s}{\partial t^m} &= 2i\gamma_e|A_p|^2A_s + i\gamma_e A_p^2A_i^* + i\gamma_f A_s\int_{-\infty}^{t} e^{-(t-t')/\tau_0}|A_p|^4dt' \\ &\quad + 2i\gamma_f A_p\int_{-\infty}^{t} e^{-(t-t')/\tau_0}e^{i\Omega_{sp}(t-t')}|A_p|^2(A_p^*A_s + A_pA_i^*)dt',\end{aligned} \tag{93}$$

$$\begin{aligned}\frac{\partial A_i}{\partial z} - i\sum_{m=0}^{\infty}\frac{i^m\beta_{mi}}{m!}\frac{\partial^m A_i}{\partial t^m} &= 2i\gamma_e|A_p|^2A_i + i\gamma_e A_p^2A_s^* + i\gamma_f A_i\int_{-\infty}^{t} e^{-(t-t')/\tau_0}|A_p|^4dt' \\ &\quad + 2i\gamma_f A_p\int_{-\infty}^{t} e^{-(t-t')/\tau_0}e^{i\Omega_{ip}(t-t')}|A_p|^2(A_p^*A_i + A_pA_s^*)dt',\end{aligned} \tag{94}$$

where we have used $\Omega_{\rm sp} = \Omega_{\rm pi}$ and kept only the first-order terms in A_s and A_i. Equations (92)–(94) show clearly that the fifth-order nonlinear effect associated with free carriers also introduce SPM, XPM, and FWM-like processes, some of which (SPM and XPM) have been discussed in preceding sections.

We now focus on a CW or quasi-CW case and assume that the pulse widths associated with the three fields are much longer than the carrier lifetime. In this case, the field amplitudes inside

#88416 - $15.00 USD Received 9 Oct 2007; revised 22 Nov 2007; accepted 25 Nov 2007; published 29 Nov 2007

the integrals in Eqs. (92)–(94) can be treated as constant, and these equations reduce to

$$\frac{\partial A_p}{\partial z} = i\beta_p A_p + i\gamma_e |A_p|^2 A_p + i\gamma_f \tau_0 |A_p|^4 A_p, \tag{95}$$

$$\frac{\partial A_s}{\partial z} = i\beta_s A_s + 2i\gamma_e |A_p|^2 A_s + i\gamma_e A_p^2 A_i^* + i\gamma_f \tau_0 |A_p|^2 \left[|A_p|^2 A_s + \frac{2}{1+i\Omega_{\rm ps}\tau_0} \left(|A_p|^2 A_s + A_p^2 A_i^* \right) \right], \tag{96}$$

$$\frac{\partial A_i}{\partial z} = i\beta_i A_i + 2i\gamma_e |A_p|^2 A_i + i\gamma_e A_p^2 A_s^* + i\gamma_f \tau_0 |A_p|^2 \left[|A_p|^2 A_i + \frac{2}{1+i\Omega_{\rm pi}\tau_0} \left(|A_p|^2 A_i + A_p^2 A_s^* \right) \right], \tag{97}$$

where $\Omega_{uv} = \omega_u - \omega_v$ $(u, v = p, s, i)$ and $\beta_v = \beta_0(\omega_v)$ is the propagation constant at the carrier frequency ω_v. Note that $\Omega_{\rm ps} = \Omega_{\rm ip}$ for a FWM process. In Eqs. (95)–(97), we have neglected linear losses and assumed pulse widths to be wide enough that all dispersive effects are negligible for individual waves.

The physical origin of various nonlinear terms in Eqs. (95)–(97) is clear. All terms involving γ_e stem from the Kerr nonlinearity, but the terms containing γ_f result from the TPA-generated free carriers. Comparing the nonlinear effects induced by these two mechanisms, we find that the efficiency of Kerr-induced FWM scales as $\gamma_e A_p^2$, but that of free-carrier-induced FWM scales as $2\gamma_f \tau_0 |A_p|^4/(1+i\Omega_{\rm ps}\tau_0)$. The relative importance of these two FWM processes is governed by the ratio

$$r_{\rm FWM} = \frac{2\gamma_f \tau_0 |A_p|^2}{\gamma_e (1+i\Omega_{\rm ps}\tau_0)}. \tag{98}$$

Noting that $\mathrm{Re}(\gamma_f) \gg \mathrm{Im}(\gamma_f)$ from Eqs. (20) and (91), and using $\gamma_e = \beta_T'(2\pi F_n + i/2) \approx 2\pi F_n \beta_T'$ for $F_n > 0.2$, where F_n is the NFOM introduced earlier, Eq. (98) can be approximated by

$$r_{\rm FWM} \approx \frac{n_0 \sigma_n \tau_0 |A_p|^2}{hcn\bar{a}F_n (1+i\Omega_{\rm ps}\tau_0)}. \tag{99}$$

As we know from nonlinear fiber optics [80], efficient Kerr-induced FWM requires $\mathrm{Re}(\gamma_e)|A_p|^2 L \sim \pi$. In a typical silicon waveguide, this condition requires a pump intensity of $|A_p|^2/\bar{a} \approx 0.4\ \mathrm{GW/cm^2}$ inside a 5-cm-long waveguide. At such power levels, $|r_{\rm FWM}| \ll 1$ when the pump-signal detuning $\Omega_{sp}/2\pi \gg 60$ GHz, since the NFOM is $F_n \approx 0.3$ in the telecom band. The magnitude of $r_{\rm FWM}$ becomes even smaller at lower pump powers. As a result, FWM induced by free carriers is negligible in most practical situations of parametric generation and wavelength conversion. However, one should keep in mind that this process could become quite efficient when pump-signal detuning becomes relatively small. For example, for a carrier lifetime of 1 ns, $|r_{\rm FWM}|$ can be larger than 250 when $|\Omega_{sp}|\tau_0 < 1$, a condition satisfied for a pump-signal detuning of $<$160 MHz.

Free carriers can affect a FWM process in another way because FWM is a coherent process and requires phase matching among the interacting waves. As free carriers introduce considerable phase modulations, they would affect the phase-matching condition of FWM. From Eqs. (95)–(97), we find that the phase mismatch induced by free carriers is given by

$$\Delta\kappa_f = \frac{4\mathrm{Re}(\gamma_f)\tau_0 |A_p|^4}{1+(\Omega_{\rm ps}\tau_0)^2}. \tag{100}$$

#88416 - $15.00 USD Received 9 Oct 2007; revised 22 Nov 2007; accepted 25 Nov 2007; published 29 Nov 2007

As the Kerr-induced phase mismatch is given by $\Delta\kappa_K = 2\mathrm{Re}(\gamma_e)|A_p|^2$, the ratio between the two is found to be

$$r_\kappa = \frac{2\mathrm{Re}(\gamma_f)\tau_0|A_p|^2}{\mathrm{Re}(\gamma_e)[1+(\Omega_{\mathrm{ps}}\tau_0)^2]}. \tag{101}$$

This expression is quite similar to Eq. (98). As a result, preceding discussion about the magnitude of r_{FWM} applies to r_κ as well. In other words, r_κ is negligible in most practical situations of parametric generation. Physically speaking, if the pump-signal detuning is not too small, free carriers impose nearly identical phase modulations on the three waves, leading to negligible phase mismatch among them, even though the absolute magnitude of such phase modulations could be large. Note that Eqs. (95)–(97) neglect the wavelength dependence of γ_f by assuming that it has the same value for all three waves. A more detailed analysis shows that free carriers do introduce some phase mismatch; this effect is discussed later. In practice, as long as the pump-signal detuning is not too small, the effects of free carriers on both FWM efficiency and phase-matching condition are negligible in the quasi-CW case, and their dominant effect comes from FCA [68].

The situation becomes quite different in the pulsed regime in which pulse widths involved become much smaller than the carrier lifetime. Although FCA is negligible in this case (as discussed earlier), transient index changes produced by free carriers can have significant impact on the FMW process. Mathematically, all the field amplitudes inside the integrals in Eqs. (92)–(94) can be considered as an ultrashort impulse, resulting in

$$\frac{\partial A_p}{\partial z} + \beta_{1p}\frac{\partial A_p}{\partial t} = i\beta_p A_p + i\gamma_e|A_p|^2A_p + i\gamma_f T_0|A_p|^4A_p, \tag{102}$$

$$\frac{\partial A_s}{\partial z} + \beta_{1s}\frac{\partial A_s}{\partial t} = i\beta_s A_s + 2i\gamma_e|A_p|^2A_s + i\gamma_e A_p^2A_i^* + i\gamma_f T_0|A_p|^2\left(3|A_p|^2A_s + 2A_p^2A_i^*\right), \tag{103}$$

$$\frac{\partial A_i}{\partial z} + \beta_{1i}\frac{\partial A_i}{\partial t} = i\beta_i A_i + 2i\gamma_e|A_p|^2A_i + i\gamma_e A_p^2A_s^* + i\gamma_f T_0|A_p|^2\left(3|A_p|^2A_i + 2A_p^2A_s^*\right), \tag{104}$$

where the pulse width T_0 is assumed to be the same for the three waves, and dispersive effects are neglected assuming that the dispersion length is longer than the waveguide length.

Following a reasoning similar to the quasi-CW case, we can find the relative impact of free carriers on the FWM efficiency and the phase mismatch through two ratios that now become

$$r_{\mathrm{FWM}} = 2\gamma_f T_0|A_p|^2/\gamma_e, \qquad r_\kappa = 2\mathrm{Re}(\gamma_f)T_0|A_p|^2/\mathrm{Re}(\gamma_e). \tag{105}$$

It turns out that the magnitude of these two ratios can become quite large in some cases. For example, it is $\sim$4 for 10-ps pulses at a 0.4 GW/cm^2 pumping level for a typical silicon waveguide. Clearly, free-carrier effects will be quite significant in this case. Note that the real part of γ_f is negative because $\sigma_n < 0$ (free carriers reduce the refractive index). As a result, with increasing pump power, free-carrier effects tends to cancel those induced by the Kerr nonlinearity, leading to a net decrease in the FWM efficiency. Moreover, the parametric bandwidth also decreases with increasing pump power. This may explain the gain saturation of parametric amplification observed experimentally with 3.5-ps pump pulses [69]. However, free-carrier effects decrease for shorter pump pulses, and may becomes negligible when the width of pump pulses is reduced to below 1 ps.

In concluding this subsection, index changes produced by free carriers have a significant impact on the FWM process for pump and signal pulses in the picosecond regime. Their impact is negligible in the quasi-CW regime in which pulse widths are much longer than the carrier lifetime. As CW pumping is required in most practical applications, we focus on this case in the following section dealing with broadband parametric generation.

#88416 - $15.00 USD Received 9 Oct 2007; revised 22 Nov 2007; accepted 25 Nov 2007; published 29 Nov 2007

5.2. *Broadband parametric generation and wavelength conversion*

One advantage of the FWM process is that its instantaneous nature supports parametric generation over a broad bandwidth. In silica fibers, parametric gain bandwidths of up to 100 nm have been demonstrated [162, 163]. In this section, we focus on FWM inside a silicon waveguide and show that, with an appropriate control of waveguide dispersion, parametric gain may be realized over a bandwidth larger than that possible for silica fibers. For a complete description of the broadband FWM process, we return to Eq. (27) rather than using Eq. (37) or (90). For simplicity, we first assume that Raman scattering does not play a significant role.

As before, the optical field is composed of three CW waves at different frequencies. substituting this form in Eq. (27), we obtain the following three equations for the pump, signal, and idler fields:

$$\frac{\partial A_p}{\partial z} = \left[i(\beta_p+\beta_p^{\rm f})-\frac{\alpha_{\rm lp}}{2}\right]A_p + i\left(\gamma_{\rm p}^e P_p + 2\gamma_{\rm ps}^e P_s + 2\gamma_{\rm pi}^e P_i\right)A_p + 2i\gamma_{\rm pspi}^e A_s A_i A_p^*, \quad (106)$$

$$\frac{\partial A_s}{\partial z} = \left[i(\beta_s+\beta_s^{\rm f})-\frac{\alpha_{\rm ls}}{2}\right]A_s + i\left(\gamma_{\rm s}^e P_s + 2\gamma_{\rm sp}^e P_p + 2\gamma_{\rm si}^e P_i\right)A_s + i\gamma_{\rm spip}^e A_p^2 A_i^*, \quad (107)$$

$$\frac{\partial A_i}{\partial z} = \left[i(\beta_i+\beta_i^{\rm f})-\frac{\alpha_{\rm li}}{2}\right]A_i + i\left(\gamma_{\rm i}^e P_i + 2\gamma_{\rm ip}^e P_p + 2\gamma_{\rm is}^e P_s\right)A_i + i\gamma_{\rm ipsp}^e A_p^2 A_s^*, \quad (108)$$

where $P_j = |A_j|^2$ for $j = s, i, p$ and the nonlinear parameters appearing in the FWM terms are obtained from Eq. (28). For example, $\gamma_{\rm pspi}^e$ is given by

$$\gamma_{\rm pspi}^e = \frac{3\omega_p \eta_{\rm pspi}\chi_{1111}^e(-\omega_p;\omega_s,-\omega_p,\omega_i)}{4\varepsilon_0 c^2 \bar{a}_{\rm pspi} n_p \sqrt{n_s n_i}}, \quad (109)$$

and $\gamma_{\rm spip}^e$ and $\gamma_{\rm ipsp}^e$ can be obtained from this equation by exchanging the subscripts. We have neglected FWM induced by free carriers because of its negligible magnitude in the CW regime.

Because of the time-reversal symmetry, the third-order susceptibilities satisfy the relation

$$\chi_{1111}^e(-\omega_s;\omega_p,-\omega_i,\omega_p) = \chi_{1111}^e(-\omega_i;\omega_p,-\omega_s,\omega_p) = [\chi_{1111}^e(-\omega_p;\omega_s,-\omega_p,\omega_i)]^*. \quad (110)$$

As a result, we find from Eq. (109) that

$$\frac{\gamma_{\rm spip}^e}{\omega_s} = \frac{\gamma_{\rm ipsp}^e}{\omega_i} = \frac{\gamma_{\rm pspi}^{e*}}{\omega_p}. \quad (111)$$

Therefore, as far as the FWM process is concerned, the last terms in Eqs. (106)–(108) lead to

$$\frac{1}{\omega_s}\frac{\partial P_s}{\partial z} = \frac{1}{\omega_i}\frac{\partial P_i}{\partial z} = -\frac{1}{2\omega_p}\frac{\partial P_p}{\partial z}. \quad (112)$$

This is the well-known Manley–Rowe relation for the FWM process, indicating the conservation of photon numbers among the three interacting waves [102, 103].

Equations (106)–(108) are quite general and include all effects related to linear loss and dispersion, nonlinear loss TPA and free carriers produced by it, various nonlinear effects (SPM, XPM, and FWM), and pump depletion. The TPA processes now become more complicated than the cases discussed earlier. The involvement of three waves leads to six possible types of TPA processes. As a result, the carrier generation rate in Eq. (36) is given by

$$\bar{G} = \sum_{v=p,s,i}\frac{\beta_{\rm Tvv}|A_p|^4}{2\hbar\omega_v \bar{a}_{\rm vv}^2} + \sum_{u,v=p,s,i}^{u\neq v}\frac{\beta_{\rm Tuv}|A_u|^2|A_v|^2}{\hbar\omega_u \bar{a}_{\rm uv}^2}, \quad (113)$$

#88416 - $15.00 USD Received 9 Oct 2007; revised 22 Nov 2007; accepted 25 Nov 2007; published 29 Nov 2007

where $\bar{a}_{\rm uv} \equiv \sqrt{a_u a_v}$ is obtained from Eq. (29).

In most practical situations, the pump is much more intense than the signal and idler fields. In this case we can ignore pump depletion as well as the SPM and XPM effects produced by the signal and idler, and Eqs. (106)–(108) reduce to

$$\frac{\partial A_p}{\partial z} = \left[i(\beta_p + \beta_p^{\rm f}) - \frac{\alpha_{\rm lp}}{2} \right] A_p + i\gamma_{\rm p}^e P_p A_p, \tag{114}$$

$$\frac{\partial A_s}{\partial z} = \left[i(\beta_s + \beta_s^{\rm f}) - \frac{\alpha_{\rm ls}}{2} \right] A_s + 2i\gamma_{\rm sp}^e P_p A_s + i\gamma_{\rm spip}^e A_p^2 A_i^*, \tag{115}$$

$$\frac{\partial A_i}{\partial z} = \left[i(\beta_i + \beta_i^{\rm f}) - \frac{\alpha_{\rm li}}{2} \right] A_i + 2i\gamma_{\rm ip}^e P_p A_i + i\gamma_{\rm ipsp}^e A_p^2 A_s^*. \tag{116}$$

As mentioned earlier, FWM requires phase matching among the interacting waves (related to momentum conservation among the four photons involved in the FWM process). From Eqs. (114)–(116), we find that the total phase mismatch is given by

$$\kappa = \Delta\beta + \Delta\beta_f + 2P_p {\rm Re}(\gamma_{\rm sp}^e + \gamma_{\rm ip}^{e*} - \gamma_{\rm p}^e), \tag{117}$$

where the first term, $\Delta\beta = \beta_s + \beta_i - 2\beta_p$, represnts linear phase mismatch, the second term, $\Delta\beta_f = {\rm Re}(\beta_s^{\rm f} + \beta_i^{\rm f} - 2\beta_p^{\rm f})$, is the phase mismatch induced by free carriers, and the last term is the nonlinear phase mismatch induced by the Kerr nonlinearity. From Eqs. (20) and (33), we find that $\beta^{\rm f}(\omega, \bar{N})$ is linearly proportional to $n_0(\omega)/\beta(\omega)$. As a result, the free-carrier-induced phase mismatch is given by

$$\Delta\beta_{\rm f} = \frac{\bar{N}\sigma_{np}\omega_p^2}{c^2}\left(\frac{n_{0s}}{\beta_s} + \frac{n_{0i}}{\beta_i} - 2\frac{n_{0p}}{\beta_p} \right) = \frac{2\bar{N}\sigma_{np}\omega_p^2}{c^2} \sum_{m=1}^{\infty} \frac{\zeta_{2m}}{(2m)!} \Omega_{\rm sp}^{2m}, \tag{118}$$

where $\zeta_m = [\partial^m (n_0 \beta^{-1})/\omega^m]_{\omega=\omega_p}$. As $\sigma_{np} < 0$, Eq. (118) shows that FCI-induced phase mismatch acts like adding negative (anomalous) second- and higher-order dispersions. The magnitudes of such equivalent GVD and fourth-order dispersion (FOD) are given by

$$\beta_2 = \bar{N}\sigma_{np}\omega_p^2 \zeta_2 / c^2, \qquad \beta_4 = \bar{N}\sigma_{np}\omega_p^2 \zeta_4 / (c^2). \tag{119}$$

However, these quantities are relatively small. For example, $\zeta_2 \sim 8 \times 10^{-13}$ m$\cdot$ps^2 and $\zeta_4 \sim 2 \times 10^{-17}$ m$\cdot$ps^4 for a typical silicon waveguide. As a result, at a pumping level of 0.4 GW/cm^2 in the telecom band, the FCI-induced GVD and FOD are about $\beta_2 \approx -0.02$ ps^2/m and $\beta_4 \approx -5 \times 10^{-7}$ ps^4/m, respectively. Both are much smaller than the GVD and FOD resulting from the waveguide confinement. Therefore, the phase-matching condition for FWM inside a silicon waveguide is dominated by the linear phase mismatch $\Delta\beta$ and the nonlinear contribution resulting from the Kerr effect.

The bandwidth of parametric gain is determined by the condition $|\kappa L| < \pi/2$. As is known from FWM in silica fibers [80, 159], it would be maximized when the pump wavelength falls close to the ZDWL of a silicon waveguide. However, the parametric bandwidth is enhanced dramatically for SOI waveguides because a typical waveguide length ($L \sim 1$ cm) is much shorter than that used for fibers. Figure 7 shows examples of the signal gain (a) and wavelength-conversion efficiency (b) for three choices of pump wavelengths for a waveguide designed with a ZDWL at 1551 nm [68]. With a proper choice of the pump wavelength, such parametric amplifiers can cover the entire so-called S, C, L, and U telecommunications bands. Similarly, if the idler is used for wavelength conversion, such wavelength converters can operate over a 300-nm bandwidth or more. Further extension of the parametric bandwidth can be realized by engineering the waveguide to reduce the impact of fourth-order dispersion. This scheme was

#88416 - $15.00 USD Received 9 Oct 2007; revised 22 Nov 2007; accepted 25 Nov 2007; published 29 Nov 2007

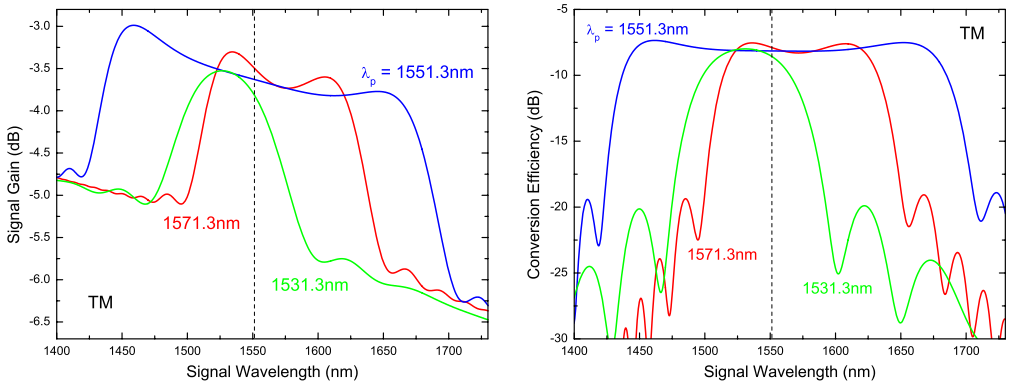

(a) (b)

Fig. 7. Signal gain (a) and wavelength-conversion efficiency (b) as a function of signal wavelength for three pump wavelengths in the vicinity of the ZDWL (dashed line) of the TM mode. Input pump intensity is 0.2 GW/cm^2 in all cases. (After Ref. [68].)

used in a recent experiment to demonstrate wavelength conversion over a bandwidth of about 150 nm [79].

Unfortunately, although the bandwidth can be made very broad through dispersion engineering, the efficiency of the FWM process is severely limited by FCA, and it is difficult to realize a net amplification with CW pumping [68]. Similar to the case of Raman amplification/lasing in Section 4.2, we can estimate the required effective carrier lifetime for parametric amplification to occur through FWM. Equations (114)–(116) show that net amplification is possible only when [68]

$$2[\mathrm{Re}(\gamma^e_{\mathrm{spip}}) - \beta'_{\mathrm{Tsp}}]P_p - \frac{n_{0s}\sigma_{as}\beta_{\mathrm{Tpp}}\tau_0 P_p^2}{2\bar{h}\omega_p n_s \bar{a}^2_{\mathrm{pp}}} - \alpha_{\mathrm{ls}} > 0, \tag{120}$$

where we have used Eq. (80) for the FCA coefficient. This inequality imposes the following upper limit on the carrier lifetime [68] :

$$\tau_0 < \frac{2\bar{h}\omega_p n_s \bar{a}^2_{\mathrm{pp}}}{\alpha_{\mathrm{ls}}\sigma_{as}n_{0s}\beta_{\mathrm{Tpp}}}[\mathrm{Re}(\gamma^e_{\mathrm{spip}}) - \beta'_{\mathrm{Tsp}}]^2 \approx \frac{2\bar{h}\omega_p n_s \beta_{\mathrm{Tpp}}}{\alpha_{\mathrm{ls}}\sigma_{as}n_{0s}}(2\pi F_n - 1)^2, \tag{121}$$

where we used $\gamma^e_{\mathrm{spip}} \approx \gamma^e_{\mathrm{p}}$, $\beta_{\mathrm{Tsp}} \approx \beta_{\mathrm{Tpp}}$, and $\bar{a}_{\mathrm{sp}} \approx \bar{a}_{\mathrm{pp}}$ in the last approximation, assuming that these quantities do not change much with the signal frequency. Equation (121) is similar to Eq. (83) obtained for Raman amplification. However, as the Kerr parameter is about 10 times smaller than the Raman gain coefficient, Eq. (121) imposes a much more stringent limit on the carrier lifetime. A detailed analysis shows that it is not possible to obtain positive parametric gain unless the carrier lifetime is reduced to below 100 ps [68]. Such a stringent requirement on carrier lifetime imposes a serious challenge to practical applications of FWM in the telecommunication band.

5.3. Coherent anti-Stokes Raman scattering

Although efficient FWM with CW pumping is difficult to realize through the Kerr nonlinearity, it turns out that amplification of the signal can occur if we take advantage of SRS. We have seen in Section 4.2 that the SRS process in silicon waveguides not only provides gain but it also introduces significant changes in the refractive index, when the pump-signal detuning lies within the Raman-gain bandwidth. Equation (88) shows that SRS introduces a maximum nonlinear

#88416 - $15.00 USD Received 9 Oct 2007; revised 22 Nov 2007; accepted 25 Nov 2007; published 29 Nov 2007

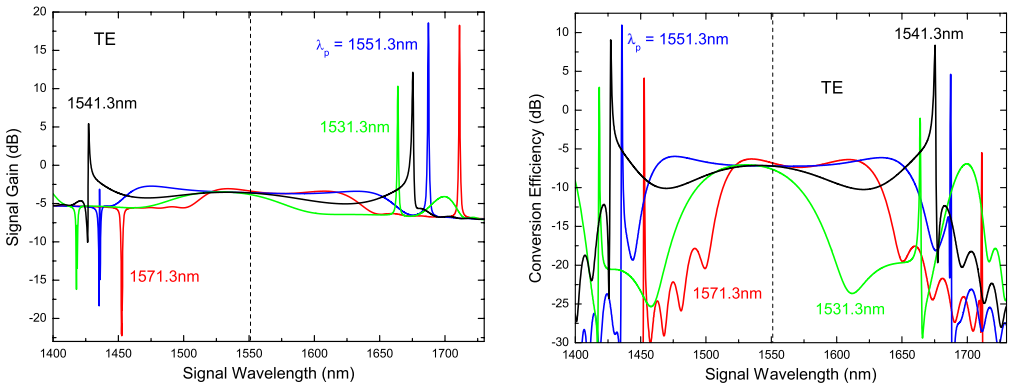

Fig. 8. Signal gain (a) and conversion efficiency (b) for the TE mode under the same conditions as in Fig. 7. (After Ref. [68].)

index change of $n_2^R \approx cg_R/(4\omega_s) \sim 1.2\times 10^{-4}$ cm^2/GW, which is much larger than that produced by the Kerr nonlinearity. As a result, when SRS contributes to the FWM process, it makes FWM much more efficient than that possible from the Kerr nonlinearity alone. This regime of FWM is known as the coherent anti-Stokes Raman scattering (CARS) process [103, 164] and is used widely for molecular spectroscopy [165]. Of course, the phase-matching condition should be maintained over the spectral region covering the Raman-gain spectrum [68].

As SRS needs to be present for this process, a specific polarization mode is required for the CARS. In the case of silicon waveguides fabricated along the $[0\ \bar{1}\ 1]$ direction, the fundamental TE mode is employed. In this situation, Eqs. (114)–(116) are replaced with the following equations to account for the Raman-induced coupling:

$$\frac{\partial A_p}{\partial z} = \left[i(\beta_p+\beta_p^{\rm f}) - \frac{\alpha_{\rm lp}}{2}\right]A_p + i\gamma_{\rm p}(0)P_pA_p, \tag{122}$$

$$\frac{\partial A_s}{\partial z} = \left[i(\beta_s+\beta_s^{\rm f}) - \frac{\alpha_{\rm ls}}{2}\right]A_s + i[\gamma_{\rm sp}(0)+\gamma_{\rm sp}(\Omega_{\rm sp})]P_pA_s + i\gamma_{\rm spip}(\Omega_{\rm sp})A_p^2A_i^*, \tag{123}$$

$$\frac{\partial A_i}{\partial z} = \left[i(\beta_i+\beta_i^{\rm f}) - \frac{\alpha_{\rm li}}{2}\right]A_i + i[\gamma_{\rm ip}(0)+\gamma_{\rm ip}(\Omega_{\rm ip})]P_pA_i + i\gamma_{\rm ipsp}(\Omega_{\rm ip})A_p^2A_s^*, \tag{124}$$

where the nonlinear parameters now include the Raman contributions, *i.e.*, $\gamma_{\rm sp}(\Omega_{\rm sp}) = \gamma_{\rm sp}^e + \gamma_{\rm sp}^R(\Omega_{\rm sp})$ and $\gamma_{\rm spip}(\Omega_{\rm sp}) = \gamma_{\rm spip}^e + \gamma_{\rm spip}^R(\Omega_{\rm sp})$.

The CARS process in silicon waveguides has been employed for wavelength conversion [61–64, 66], but its efficiency was relatively low. The reason turns out to be the phase-matching condition [68]: CARS can become efficient only when phase matching is realized for a signal separated from the pump by the Raman shift of 15.6 THz. This can be realized by choosing the pump wavelength appropriately with respect to the ZDWL of an SOI waveguide [68]. Figure 8 shows the signal gain and wavelength-conversion efficiency as a function of signal wavelength under conditions similar to those used for Figure 7, except that the Raman-induced enhancement of the FWM process is included. As seen there, by choosing the pump wavelength in the normal-dispersion region of the waveguide, the phase matching condition can be satisfied for the Stokes and anti-Stokes waves, leading to a positive gain of about 9 dB, even with CW pumping.

#88416 - $15.00 USD Received 9 Oct 2007; revised 22 Nov 2007; accepted 25 Nov 2007; published 29 Nov 2007

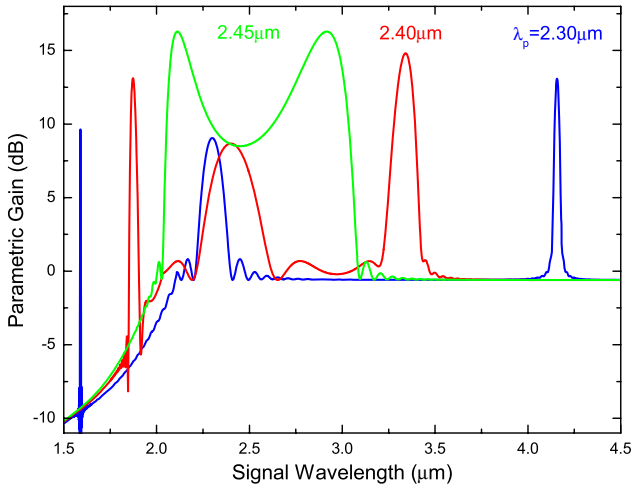

Fig. 9. Parametric gain spectra at three pump wavelengths in the mid-infrared region for the waveguide with a cross section of $1.8 \times 0.4\ \mu\text{m}^2$. (After Ref. [137].)

5.4. *Highly tunable parametric generation from the telecom band to the mid-infrared*

Although the CARS process enables positive parametric gain, its spectral location is fixed within the Raman gain bandwidth. To take advantage of the instantaneous nature of FWM outside this spectral region, we should go back to the Kerr nonlinearity and ask what limits the FWM efficiency in the CW regime used for Figure 7. As we have seen, it is the presence of losses induced by the free carriers (FCA). Recalling that free carriers are created through TPA, it is immediately obvious that the FWM efficiency can be improved drastically by choosing the pump wavelength beyond 2.2 μm. As the pump wavelength then falls below the half-band gap of silicon, TPA vanishes [83, 84], and efficient parametric generation becomes possible. Note that the signal wavelength can still be well above the half band gap, if the SOI waveguide is designed properly to satisfy the phase-matching condition over a wide bandwidth [137].

Figure 9 shows an example of such a FWM configuration. By tailoring the ZDWL of the fundamental TE mode to 2349 nm using a waveguide cross section of $1.8 \times 0.4\ \mu\text{m}^2$, parametric amplification becomes very efficient when pump wavelength is located in the vicinity of ZDWL because no TPA can occur. For example, a broadband gain spectrum with positive gain is obtained at a pump wavelength of 2.45 μm falling in the anomalous-GVD regime. Even when the pump wavelength falls in the normal-GVD regime, higher-order dispersive effects can assist in satisfying the phase-matching condition to provide gain in spectral regions far from the pump. In this regime, phase matching becomes very sensitive to the pump wavelength. The main point to note is that efficient parametric amplification is possible at signal wavelengths extending from 1.5 μm to mid infrared by simply tuning the pump wavelength within 100 nm. Tunability of the signal is more than 5 times larger than the pump itself. Although it was proposed recently to use silicon Raman laser in mid infrared [166], its lasing frequency is fixed with respect to the pump. In contrast, the FWM-based parametric amplification discussed here can provide a much larger bandwidth and broader tunability, features comparable with those available in $\chi^{(2)}$ materials such as a periodically poled lithium-niobate waveguide.

5.5. *Photon pair generation by FWM*

So far, we have focused on the traditional regime in which a high-power pump is used to amplify a signal and simultaneously generate an idler beam. However, as FWM is a four-photon elastic

#88416 - $15.00 USD Received 9 Oct 2007; revised 22 Nov 2007; accepted 25 Nov 2007; published 29 Nov 2007

scattering process, it conserves physical quantities, such as energy and momentum, among the four interacting photons. As a result, if no signal is initially present so that FWM is initiated from vacuum noise, and the pump power is relatively low so that stimulated FWM does not occur, it is possible to create only one pair of signal and idler photons at a time (within the coherence time of the pump) that are correlated quantum mechanically in multiple dimensions. Such correlated photon pairs are useful for applications in quantum information processing. Indeed, spontaneous FWM in silica fibers have been used for this purpose successfully in the past few years [167–170].

Unfortunately, pump photons also interact with thermal phonons and generate uncorrelated signal/idler photons through spontaneous Raman scattering (SpRS). This process is found to impose a severe limit on the degree of the quantum correlation between the signal and idler photons [171–173]. Because of the broadband nature of SpRS in silica fibers, high-quality correlated photon pairs can be generated only at frequencies far from the pump (>25 THz) [169, 170]. They can also be generated within the Raman-gain bandwidth by cooling the fiber with liquid nitrogen [174,175]. The SpRS problem can also be solved using silicon waveguides. As we have seen earlier, Raman scattering in a silicon crystal occurs only for specific polarizations within a very narrow (105-GHz wide) band and can easily be avoided. For this reason, if spontaneous FWM inside a silicon waveguide is used to create correlated photon pairs, photon pairs should have a very high quality [73].

In the low-power regime, pump depletion can be neglected completely, and the pump wave is described classically by Eq. (122). However, the signal and idler waves must be treated quantum mechanically. Equations (123) and (124) should thus be replaced by the corresponding operator equations, as was done first in a 2006 study [73], resulting in the following signal equation:

$$\frac{\partial \hat{A}_s}{\partial z} = [i(\beta_s + \beta_s^{\mathrm{f}}) - \frac{1}{2}\alpha_{\mathrm{ls}}]\hat{A}_s + i[\gamma_{\mathrm{sp}}(0) + \gamma_{\mathrm{sp}}(\Omega_{\mathrm{sp}})]P_p\hat{A}_s + i\gamma_{\mathrm{spip}}(\Omega_{\mathrm{sp}})A_p^2\hat{A}_i^\dagger + \hat{m}_l(z,\omega_s) + \hat{m}_f(z,\omega_s) + \hat{m}_T(z,\omega_s)A_p + i\hat{m}_R(z,\Omega_{\mathrm{sp}})A_p. \quad (125)$$

The idler equation can be obtained by exchanging the subscripts s and i. The four noise operators (last 4 terms) in Eq. (125) are associated with scattering losses, FCA, TPA, and Raman gain/loss, respectively. They obey a commutation relation of the form

$$[\hat{m}_j(z_1,\omega_u), \hat{m}_j^\dagger(z_2,\omega_v)] = 2\pi D_j \delta(\omega_u - \omega_v)\delta(z_1 - z_2), \quad (126)$$

where D_j ($j = l, f, T, R$) stands for $\alpha_l(\omega_u)$, $\alpha_{\mathrm{f}}(z_1,\omega_u)$, $2\beta'_{\mathrm{Tup}}$, and $g_R(\Omega_{\mathrm{up}})/\bar{a}_{\mathrm{up}}$ for the four noise sources, respectively. In the case of SpRS, the photon frequency ω in Eq. (126) is replaced with the phonon frequency $\Omega = \omega - \omega_p$.

Equation (125) together with Eqs. (122) and (126) can be used to find the photon generation rate and the quantum correlation between the signal and idler photons [73]. An example is shown in Fig. 10. A detailed analysis shows that FCA and TPA play minor roles because of the low pump power used. Thus, FWM in silicon waveguides is quite efficient for photon-pair generation. Such a silicon-base scheme not only provides a pair correlation close to the fundamental limit set by a pure FWM process but also exhibits a spectral brightness that is comparable to other photon-pair sources. This scheme has recently been used to generate correlated photon pairs [75], and a maximum coincidence-to-accidental ratio of 25 was obtained at a photon production rate of 0.05 per pulse. This value is still far below the predicted theoretical value, indicating room for future improvement.

6. Summary

Several kinds of nonlinear optical effects have been observed in silicon waveguides in recent years, and their device applications are attracting considerably attention. In this review, we have

#88416 - $15.00 USD Received 9 Oct 2007; revised 22 Nov 2007; accepted 25 Nov 2007; published 29 Nov 2007

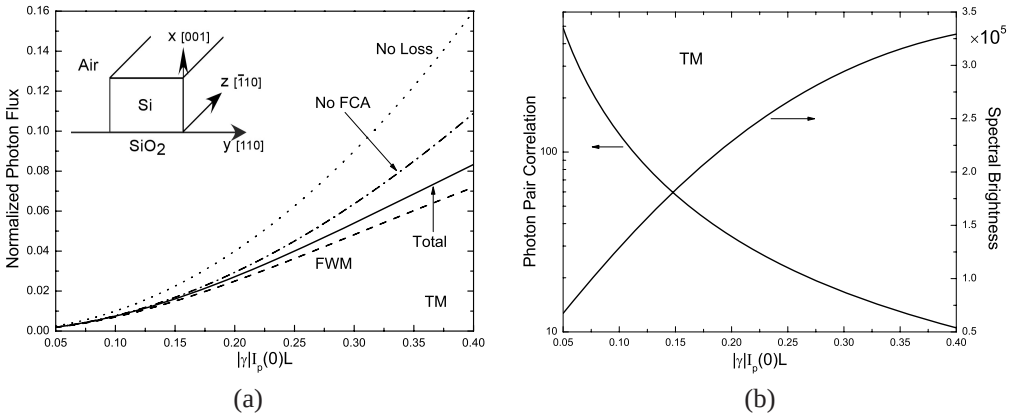

Fig. 10. Normalized photon flux (a) and pair correlation and spectral brightness (b) for the TM mode as a function of pump intensity. The inset shows the waveguide design. (After Ref. [73].)

provided a unified theoretical platform that can be used not only for understanding the underlying physics but also to provide guidance toward new and useful applications. We began in Section 2 with a description of the third-order nonlinearity of silicon and considered the tensorial nature of both the electronic and Raman contributions. The generation of free carriers through TPA and their impact on various nonlinear phenomena is included fully in the theory presented here. We derived a general propagation equation in the frequency domain and showed how it leads to a generalized nonlinear Schrödinger equation when it is converted to the time domain. We used this equation to study propagation of ultrashort optical pulses in the presence of SPM and showed the possibility of soliton formation and supercontinuum generation. The nonlinear phenomena of XPM and SRS were discussed next in a separate section, with emphasis on the impact of free carriers on Raman amplification and lasing. Section 5 focused on the FWM process and its applications. We considered first the impact of free carriers and showed that, although index changes induced by them have a negligible impact on FWM, FCA limits the FWM efficiency so much that a net positive gain cannot be realized in the telecommunication band in the case of CW pumping. However, this problem can be solved by pumping at wavelengths beyond 2.2 μm because TPA-induced free carriers are then absent. We also showed that FWM can occur over a wide bandwidth, with a proper choice of the pump wavelength, because of much smaller waveguide lengths employed compared with those required for silica fibers. We also discussed briefly the use of FWM in silicon waveguides for generating correlated photon pairs that are useful for quantum applications.

Acknowledgements

The authors thank P. M. Fauchet, R. W. Boyd, T. E Murphy, J. Zhang, G. Piredda, L. Yin, T. J. Johnson, R. Perahia, and C. P. Michael for helpful discussions. This work was supported in part by the National Science Foundation, Air Force Research Office, and DARPA EPIC program.

#88416 - $15.00 USD Received 9 Oct 2007; revised 22 Nov 2007; accepted 25 Nov 2007; published 29 Nov 2007